ADVANCED MATERIALS

Supporting Information

for *Adv. Mater.,* DOI: 10.1002/adma.201502047

An Ultrahigh Pore Volume Drives Up the Amine Stability and Cyclic CO_2 Capacity of a Solid-Amine@Carbon Sorbent

Srinivas Gadipelli, Hasmukh A. Patel, and Zhengxiao Guo**

Supporting Information

Ultrahigh Pore Volume Drives up Amine Stability and Cyclic CO_2 Capacity of a Solid Amine@Carbon Sorbent

Srinivas Gadipelli, Hasmukh A. Patel, and Zhengxiao Guo**

Sample Synthesis:

MOF-5: The millimeter sized MOF-5 crystals were synthesized and activated according to the literature.[23,35] Briefly, 6.3 g of zinc nitrate tetrahydrate (Merck) and 1.35 g of terephthalic acid (Aldrich) were dissolved in 300 ml of freshly distilled *N, N*-diethylformamide (DEF, Acros) in a 500 ml wide mouth glass jar (Fisherbrand) with screw tight cap. The tightly sealed glass jar was then left in an oven for 2 days at 100 °C. The MOF crystals were activated by first decanting the mother liquor, washing with DEF, and finally immersing them in chloroform (Fisher). The exchange solvent was refreshed 5 times during 5 day period.

MDCM: The MDCM was obtained by direct carbonization of MOF-5.[23,25] In the carbonization process, about 500 mg of MOF-5 placed in an alumina boat, 1.0 cm × 1.5 cm × 5 cm and transferred into a horizontal tube furnace. The furnace tube was closed with a gas feedthrough end seals and sample area was thoroughly purged with nitrogen. The nitrogen flow was maintained throughout the reaction, about 24 h. The carbonization was carried out at 1000 °C with a dwelling time of 6 h after a heating with 5 °C/min. Thus obtained carbon is named as MDCM and was used as such for further characterizations and amine impregnation with any further treatment.

ActGO: The ActGO was synthesized according to the literature.[36] Briefly, the exfoliated graphene-oxide (GO) (at 250 °C, synthesized by Hummers' method) (400 mg) was soaked in 20 ml KOH (7 M) solution overnight. The solution was then removed by filtration and dried at 100 °C. The solid was then transferred in to a tube furnace and activated at 800 °C for an hour after heating at a rate of 3 °C/min under N_2 flow. After the activation, the sample was washed with distilled water until the pH value of reached 7 and dried.

TEPA: Purchased form Sigma-Aldrich (technical grade). It has a low toxicity and exhibits high amine concentration for interacting with CO_2 over PEI (40% over 27.5% primary and secondary amines for CO_2).

Typically, active alkali $–NH_2$ group possess lone a pair of electrons on N atom which undergoes nucleophilic attack on the C atom of acidic CO_2, resulting in carbamate formation through carboxyl group. The active H atom in carboxyl group may then form ion pairs through hydrogen bond with the nearby amine group/moisture in feed gas, and thus stabilizes the chemisorption of CO_2.[32]

Brönsted acid-base reaction,

$R-NH_2+CO_2 \Leftrightarrow R-NH-COOH$, yielding a carbamic acid

$R-NH_2+CO_2+H_2O \Leftrightarrow R-NH_3^+ + HCO_3^-$, yielding an ammonium hydrogen-carbonate ion pair or H_2CO_3 forms.

Amine@MOF-5, MDCM & ActGO: TEPA impregnation was carried out with methanol (Merck) solution blending. The required amount of amine (between 2 to 6 times the weight of MDCM) was carefully added to the already weighed MOF-5, MDCM & ActGO from the amine-methanol stock solution and later these solid-solution mixtures were aged for several hours on a shaker. All these sample handling was done at room temperature and ambient air. The sample vials then transferred to an air tight vacuum oven and left at 60 °C and up to a day to dry the samples. The amine loading was estimated from the initial and final dry sample weights. The samples were labelled according to the amine loading with respect to the MDCM. Example, 4.0TEPA@MDCM represents the 400 mg TEPA loading for a 100 mg MDCM, i.e., equal to 80% loading.

Characterizations:

Powder X-ray diffraction (PXRD, on Stoe Stadi-P, Cu-K-alpha) was carried out by filling the sample in a 1.0 mm diameter glass capillary at ambient. X-ray Photoemission spectroscopy (XPS, on Al-K-alpha, Thermo Scientific) data were obtained on the samples depositing on carbon tape. Fourier-transform Infrared (FTIR, on Nicolet 6700 FTIR) data was obtained at room temperature by KBr pellet transmission method with background correction. Raman spectra and optical images were recorded with 514.5 nm laser and ×50 microscope (Renishaw) on the pressed sample powders on glass slide. Scanning electron microscopy (SEM, Jeol) and transmission electron microscopy (TEM, Jeol) images were obtained on the samples deposited on the carbon tape and carbon coated TEM copper grid. The surface area and pore volume values for all the samples were obtained from nitrogen adsorption-desorption isotherms, measured at 77 K on Quantachrome Autosorb-iQC. The specific surface area was measured from the isotherm in the relative pressure range between 0.01 and 0.25, according to the Brunauer-Emmett-Teller (BET) method. QSDFT (quenched solid density functional theory) method with slit/cylindrical pores (≤50 nm) is applied to obtain pore size distribution, micropore volume and cumulative pore volume. BJH method was applied to estimate meso (>3nm) and macropores (>50 nm). The total pore volume was estimated from the amount of N_2 adsorbed at a relative pressure of ~0.99. Note that the total pore volume at P/Po = ~0.99 is fairly in good agreement with the total pore volume obtained through BJH method (meso+macro) + QSDFT method (micro).

The thermogravimetric (TG, on Setsys from Setaram) analysis was carried out under Ar flow. The sample was left at 100 °C for 50 min for degassing of adsorbed CO_2 and moisture, a heating rate of 5 °C/min was maintained. The TG mass-loss was recorded after background correction to empty alumina crucible.

For CO_2 uptake, all the samples were initially screened with volumetric adsorption isotherms using a dry, 100% CO_2 (Research grade, purchased from BOC, UK) and measured up to 1 bar and up to 75 °C (maintained by water bath) on a Quantachrome Autosorb-iQC. The sample was degassed at 70 °C prior to the actual CO_2 adsorption isotherm measurement.

The cycling CO_2 uptake was determined by gravimetric method on TG under flowing gas at 50 ml min^{-1} around 1 bar. The tests were carried out with 3 different conditions of the test gas; 1) humidified (bubbled through water bubbler) 15% CO_2 balanced with 85% N_2 (purchased from BOC, UK), 2) humidified 100% CO_2, 3) humidified 100% N_2, as reference. In each case the CO_2 desorption cycle was obtained with a dry, 100 N_2 flow (50 ml min^{-1}) at ~100 °C. The sorption tests were conducted at (60-90) °C. As experiment involved switching between the gases for each sorption and desorption run, the measurements were carried out in a day time and left with CO_2 overnight at room temperature to start the following cycling next day.

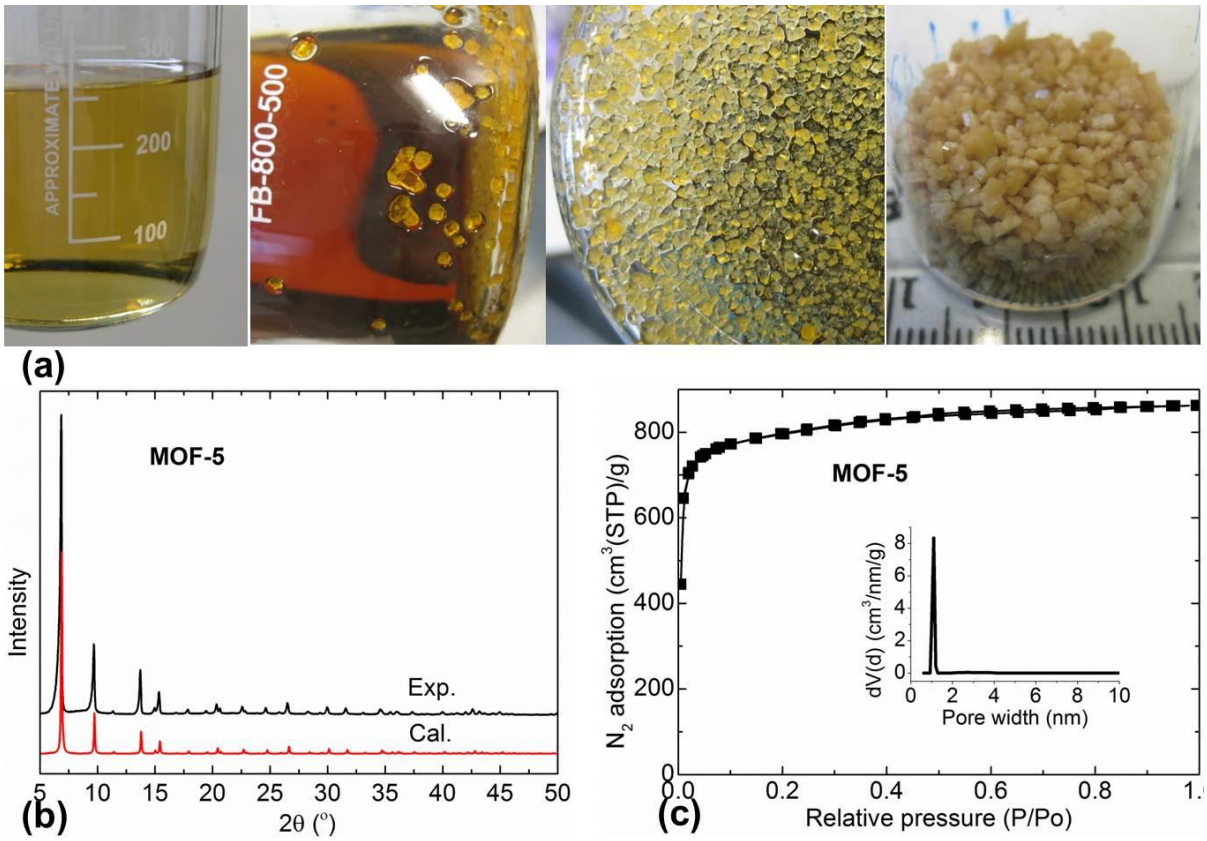

Figure S1. (a) Digital photographs of MOF-5 during its synthesis in a wide mouth 500 ml screw cap glass bottle. From left to right: Precursors dissolved in a DEF, MOF-5 crystals precipitated from solution after heat treated at 100 °C for 2 days, the surface grown crystals after decanting DEF and rinsing with chloroform and a final dry product collected in a glass vial. The scale shows (1–2) nm sized crystals. (b) PXRD pattern of MOF-5; experimental and calculated are represented by black and red in colour, respectively. (c) N_2 adsorption isotherm of MOF-5 was measured at 77 K, yielding a BET specific surface area of 3170 $m^2 g^{-1}$ and pore volume of 1.33 $cm^3 g^{-1}$, in good agreement with the literature.[35] Inset: a pore size distribution plot showing a single pore around 1.1 nm, deduced from the isotherm data by applying NLDFT method.

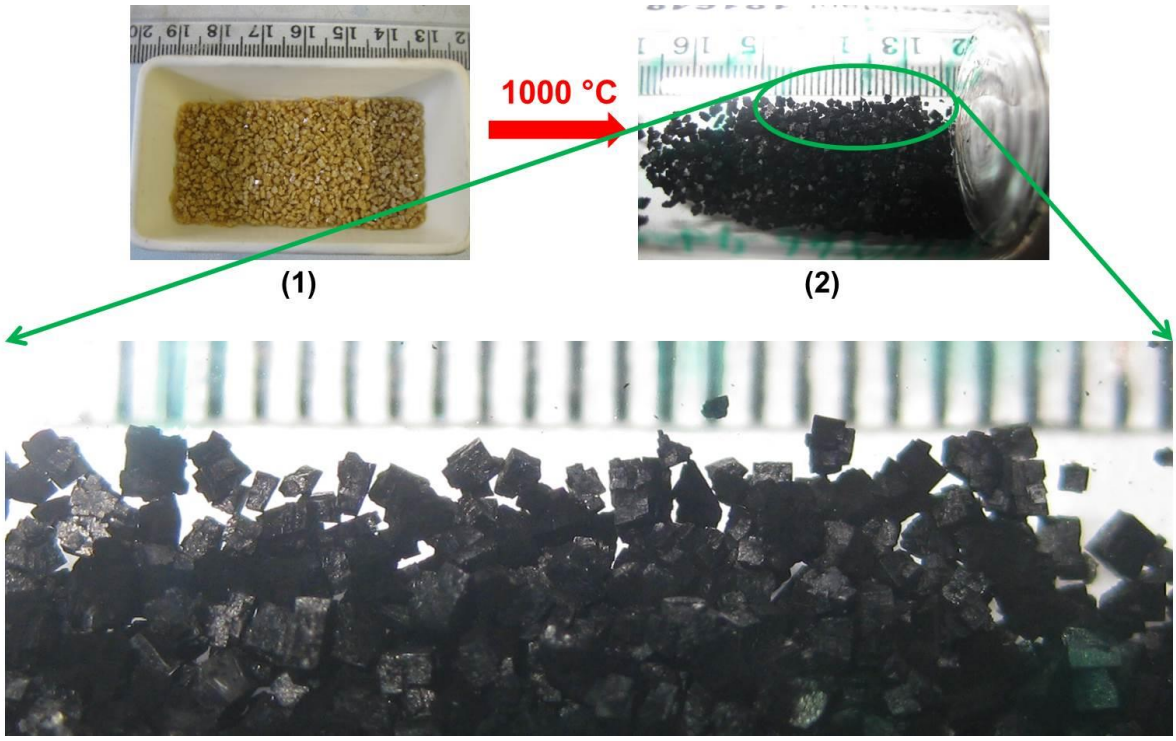

Figure S2. Carbonization of MOF-5; the digital photographs of (1) MOF-5 crystals in an alumina boat and (2) a 1000 °C carbonized MOF-5 sample in a glass vial. The bottom picture shows the magnified view of the (2), where a millimeter sized carbon monoliths are clearly seen. The MOF-5 crystallites remain after carbonization (also see Ref. [23,25]).

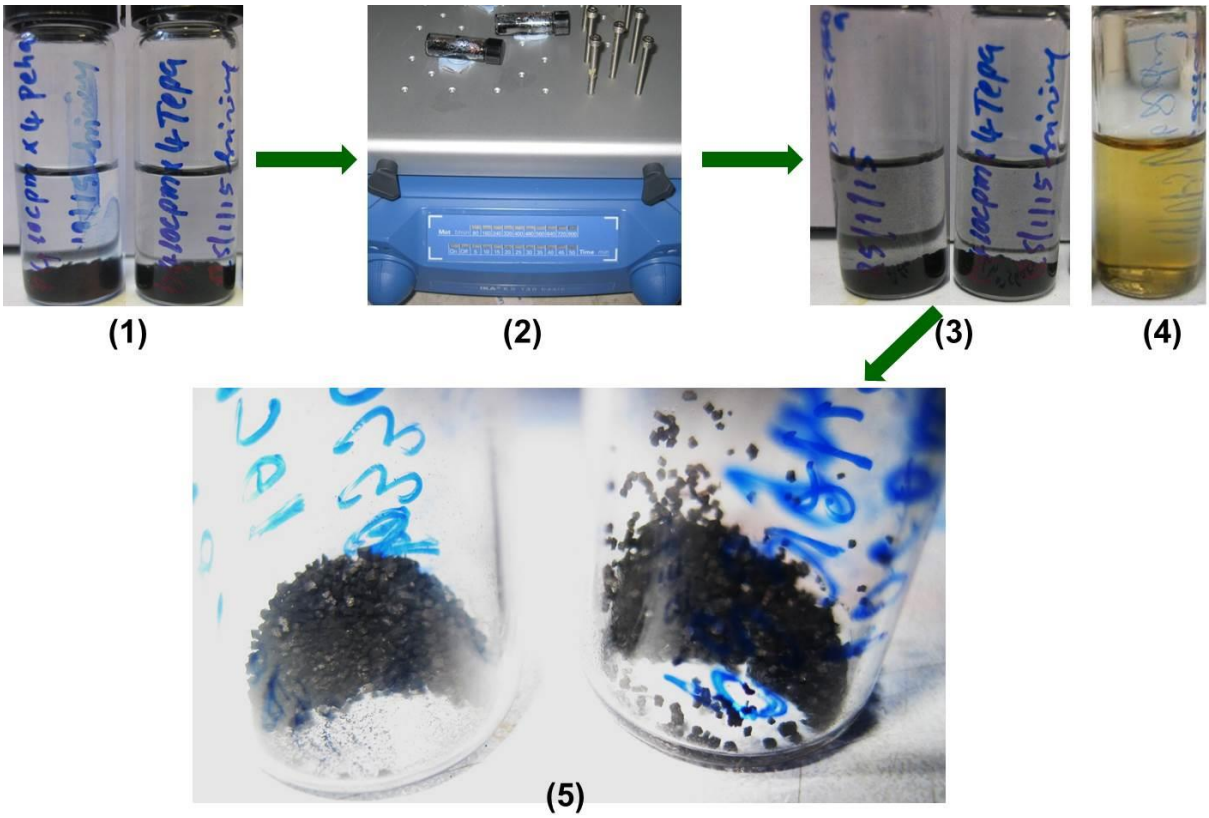

Figure S3. Synthesis of TEPA@(MOF-5 and MDCM); the digital photographs of (1) MDCM in a TEPA-methanol solution, (2) homogenized on shaker at 300 min^{-1} for several hours, (3) after removed from shaker, a clear solution suggest that MDCM remains same without disintegrating it into powder form as shown in (5) after drying the sample under rotary vacuum at 60 °C. (4) a dissolved MOF-5 showing yellowish solution from its initial clear TEPA-methanol solution.

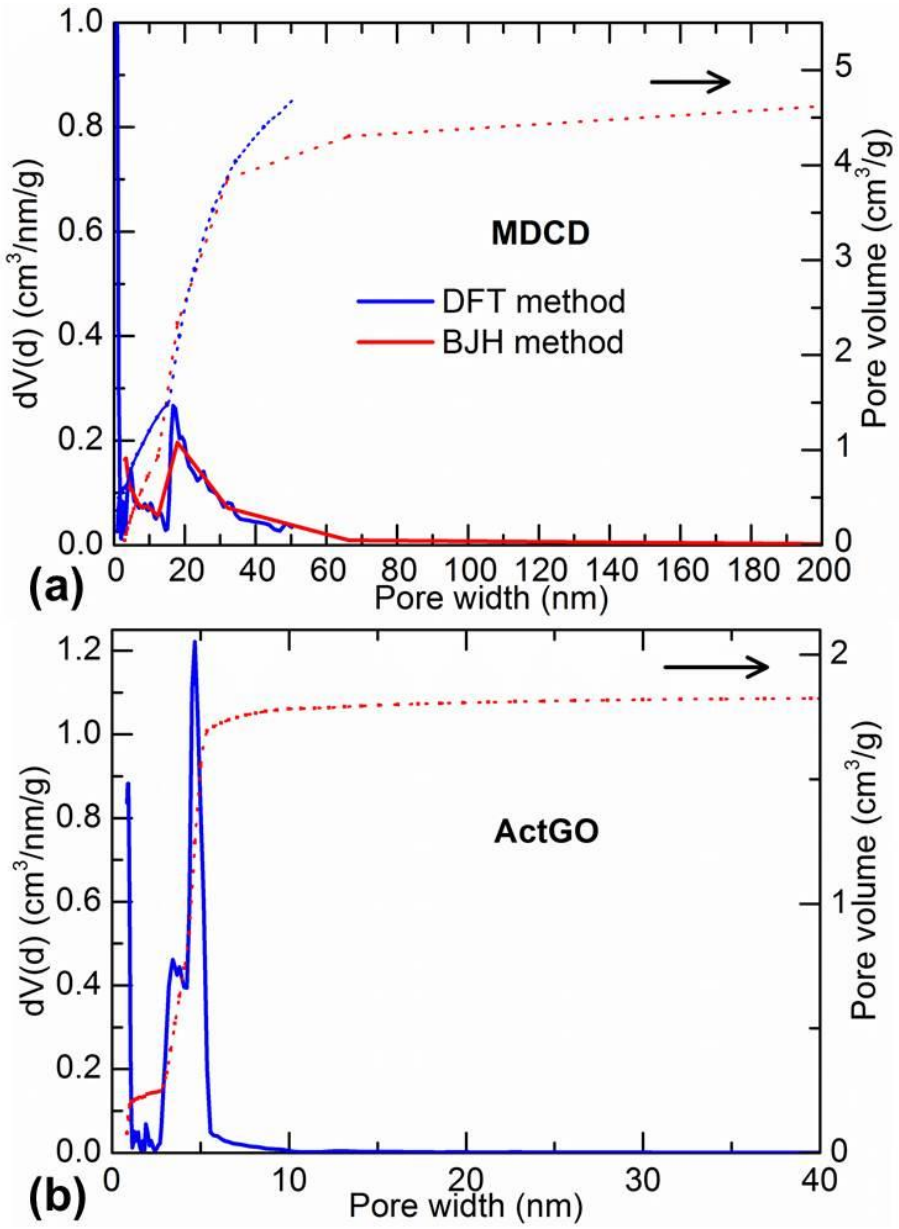

Figure S4. A full range PSD (solid line) and V_p (dotted line) plots of (a) MDCM and (b) ActGO, obtained by fitting the 77 K nitrogen desorption isotherm with QSDFT (up to 50 nm) and BJH models. For MDCM, both models are in good agreement and show that most of the mesoporosity is centered at ~20 nm with a broad distribution of hierarchical mesopores between (2–60) nm. The cumulative pore volume for narrow/slit pore of ≤3 nm accounts ~0.6 $cm^3\ g^{-1}$, whereas BJH estimates about 4.65 $cm^3\ g^{-1}$ mesoporosity for the pores ≥3 nm. Overall the DFT and BJH total pore volume, ~5.25 $cm^3\ g^{-1}$ (0.6 + 4.65) is in good agreement with the nitrogen isotherm derived total pore volume of 5.35 $cm^3\ g^{-1}$. Which is a simple relation, defined as, total pore volume = (N_2 adsorbed at 0.99 in $cm^3\ g^{-1}$) × (N_2 gas density at STP)/(N_2 liquid density at ~1 bar). That is nothing but, $V_p = V_{ads}$ at (P/Po=0.99) × 0.001547.
In ActGO the majority of pores are situated at ≤5 nm with a narrow distribution between (2–10) nm. Again the DFT estimated pore volume, ~1.8 $cm^3\ g^{-1}$ is in good agreement with the nitrogen isotherm derived total pore volume, ~1.95 $cm^3\ g^{-1}$.

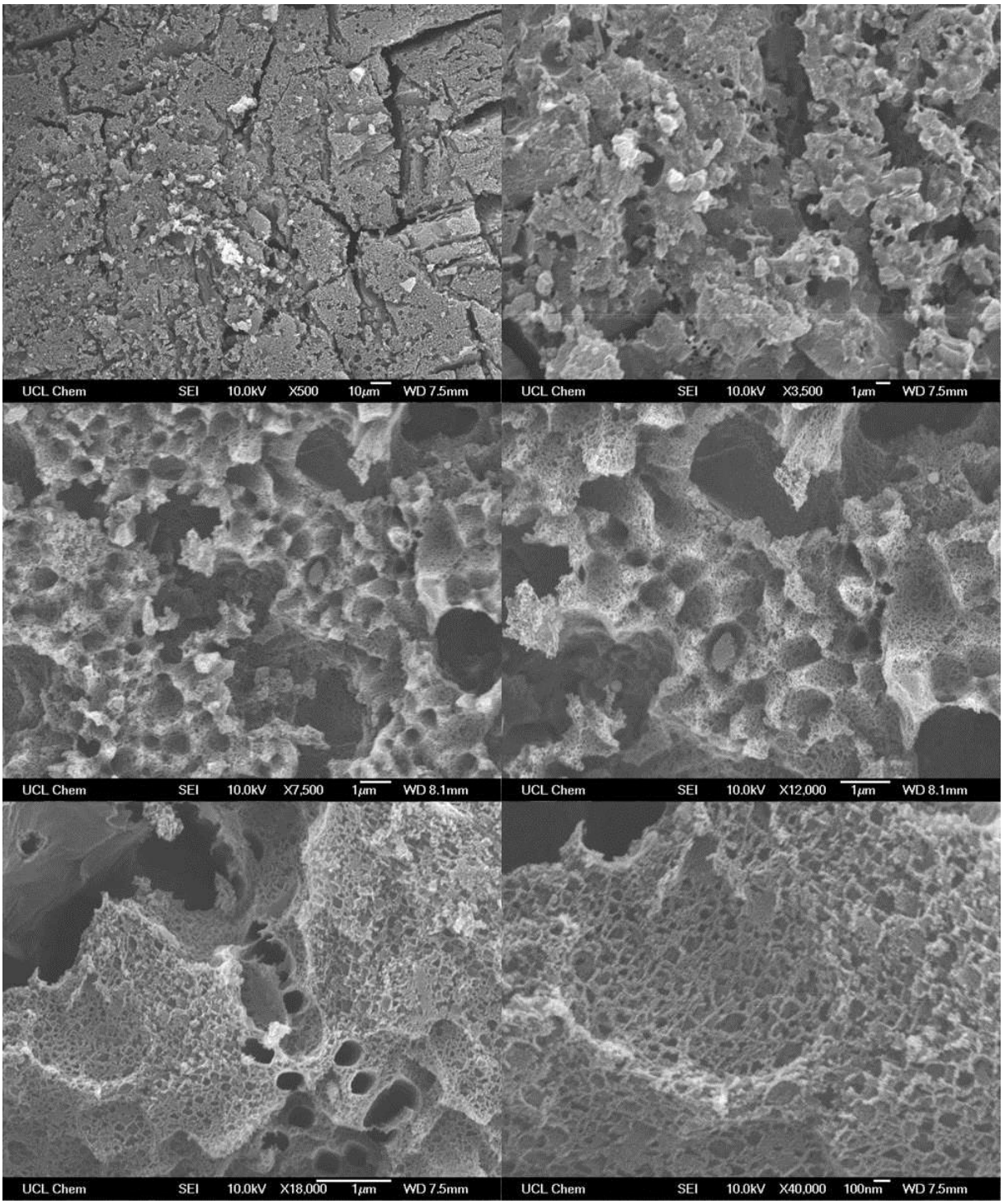

Figure S5a. Low and high magnification SEM images of MDCM. For more clarity SEM images were recorded after breaking down a MDCM to smaller particles by gentle crushing.

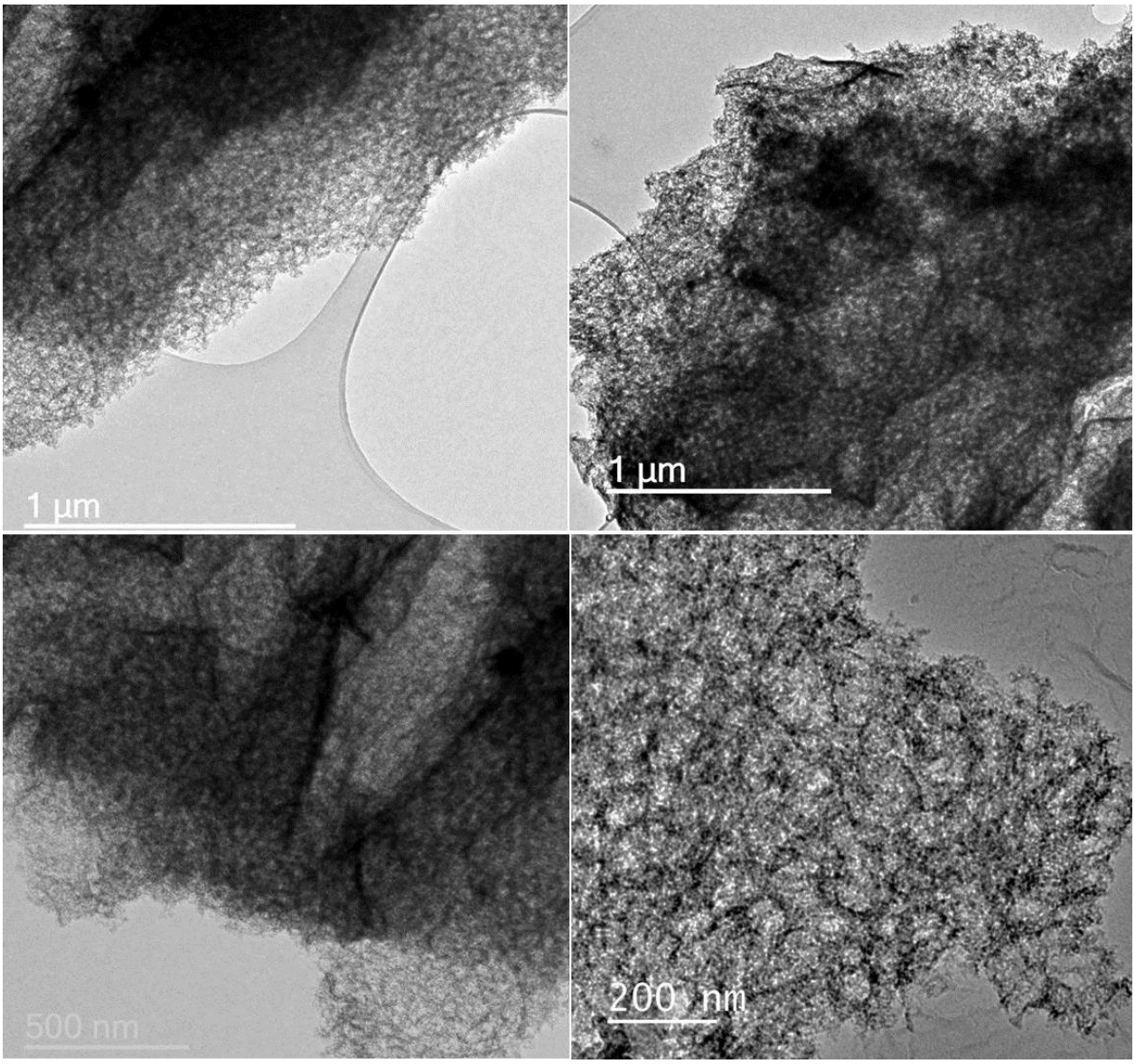

Figuire S5b. TEM images of MDCM were obtained on crushed powder and dispersed in methanol.

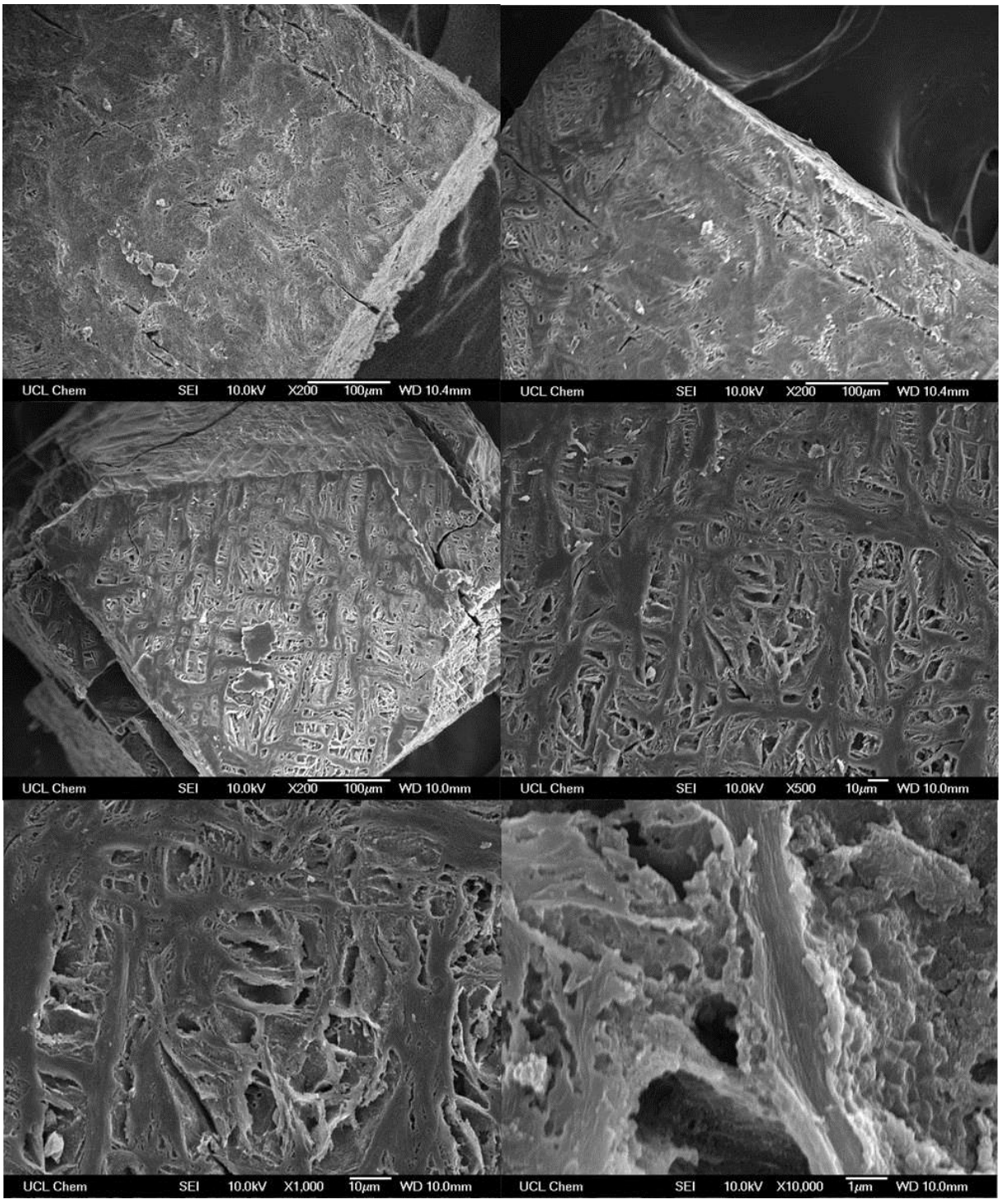

Figure S5c. Low and high magnification SEM images of 4.0TEPA@MDCM.

Table S1. The porosity characteristics of MOF-5, MDCM, ActGO and TEPA loaded samples.

S. No.	Sample	BET specific surface area ($m^2 g^{-1}$)	Total pore volume ($cm^3 g^{-1}$)
1	MOF-5	3170	1.33
2	MDCM	2700	5.35
3	ActGO	2445	1.95
4	2.0TEPA@MDCM	134	0.76
5	3.2TEPA@MDCM	112	0.46
6	3.6TEPA@MDCM	40	0.29
7	4.0TEPA@MDCM	27	0.17
8	5.0TEPA@MDCM	18	0.03
9	6.0TEPA@MDCM	6	0.01
10	1.8TEPA@ActGO	38	0.06
11	2.3TEPA@ActGO	24	0.03
12	3.3TEPA@ActGO	30	0.02
13	4.4TEPA@ActGO	20	0.01

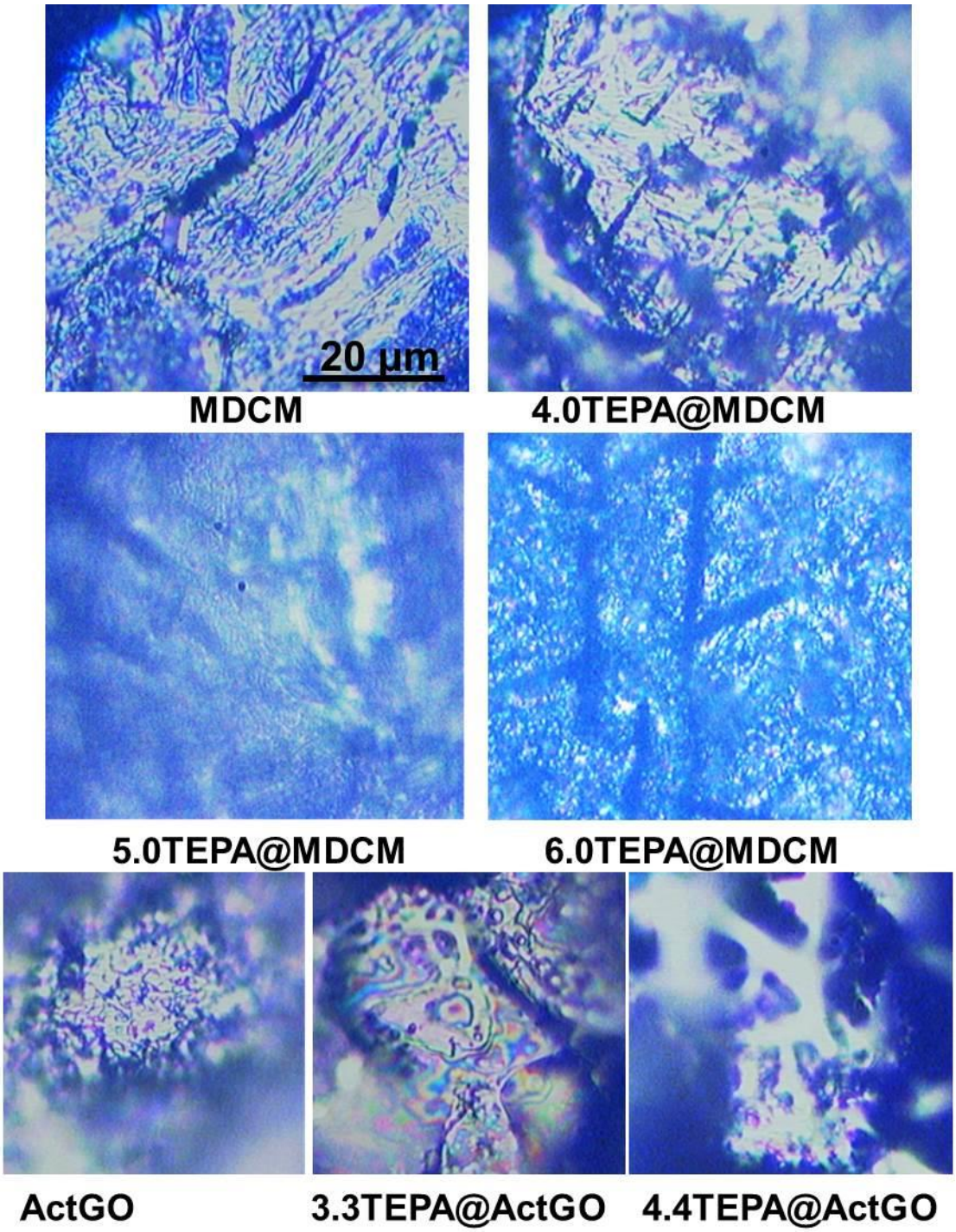

Figure S6. Optical images of MDCM and ActGO before and after TEPA loading at different levels were taken on the Raman kit with a ×50 microscope.

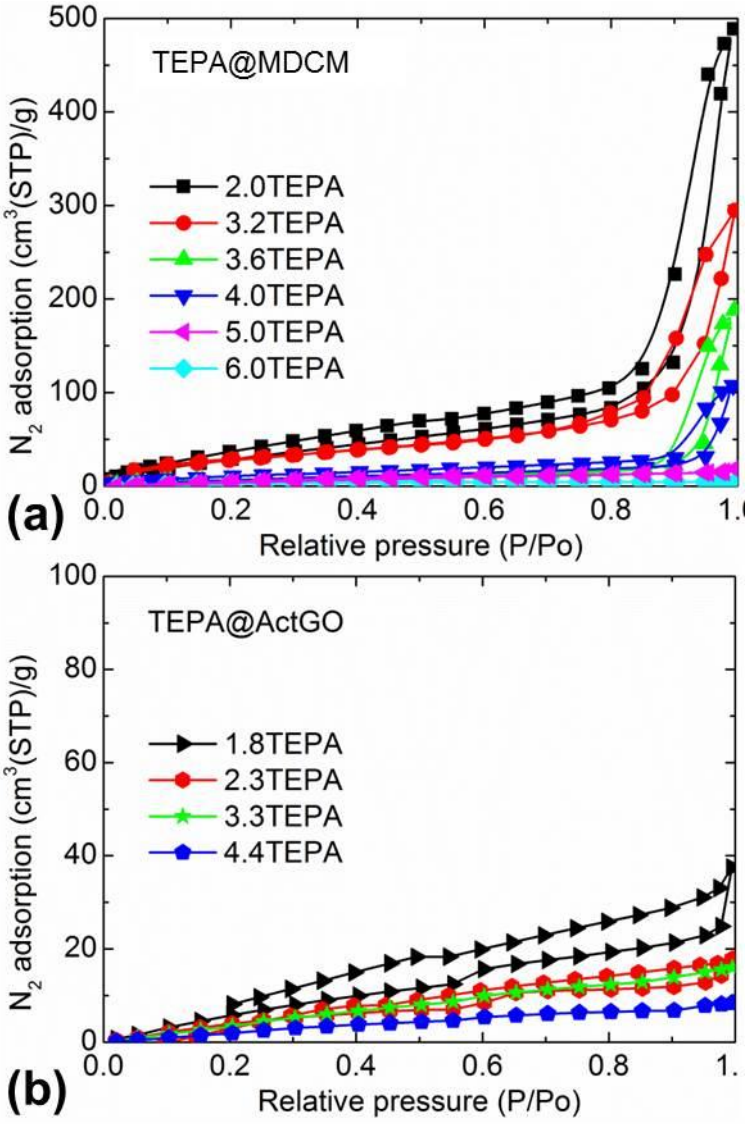

Figure S7. 77 K nitrogen isotherms as a function of TEPA loading in (a) TEPA@MDCM and (b) TEPA@ActGO. Clearly MDCM shows relatively much higher free pore space compared with complete pore filling in ActGO for given the same amount of TEPA loading.

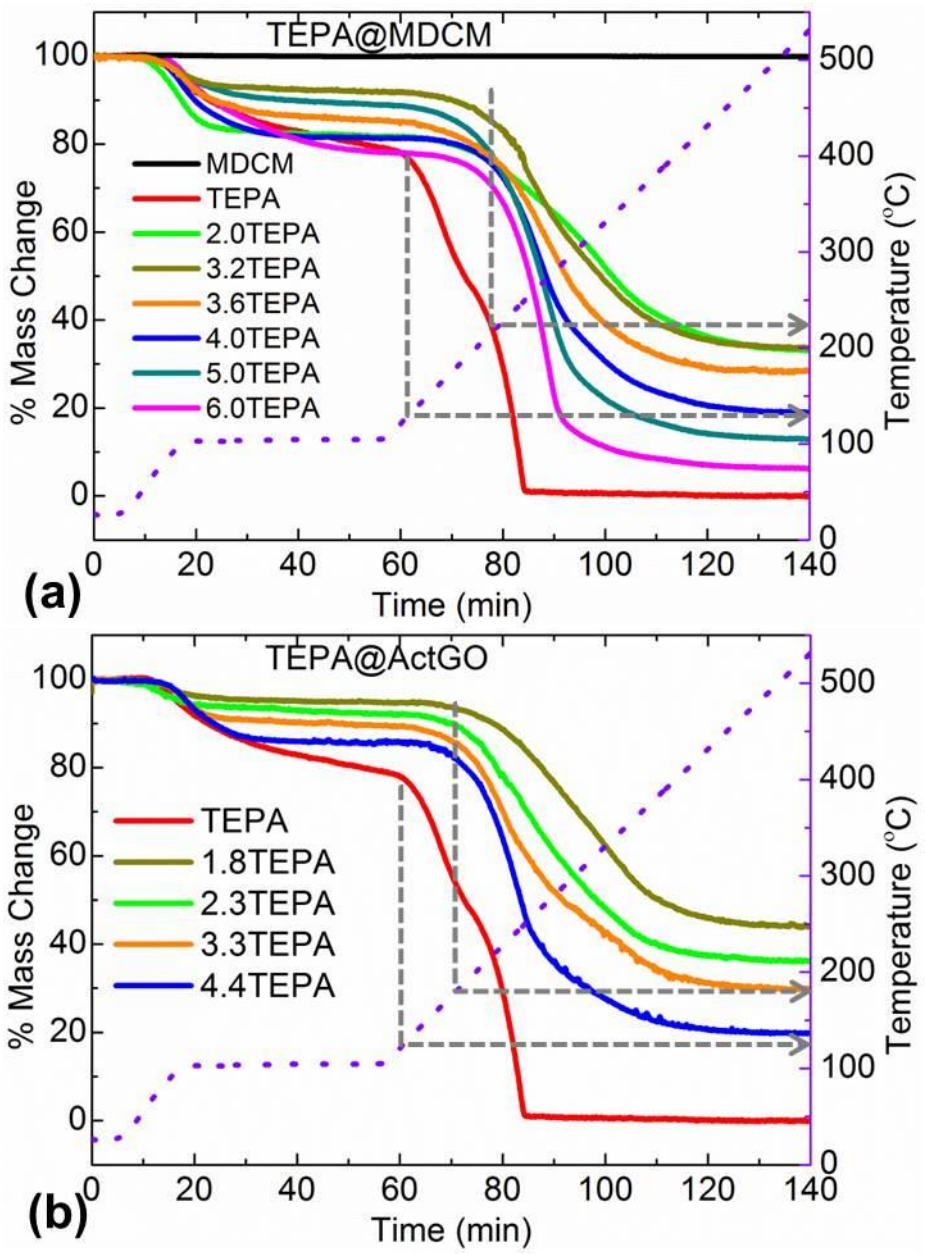

Figure S8. TG plots of (a) TEPA@MCDM and (b) TEPA@ActGO. For a reference, host MDCM and bulk TEPA is also measured with a heating rate of 5 °C min^{-1} and 50 minute isothermal step at 100 °C. The mass loss at ≥200 °C is due to TEPA decomposition. The initial small mass-loss between (25–100) °C could be attributed to the removal of moisture and pre-adsorbed CO_2. Clearly a high thermal stability of TEPA is observed in both when impregnated in MCDM and ActGO than bulk TEPA. Due to high content of hierarchical pore volume in MDCM the TEPA@MDCM carbon shows highest thermal stability of nearly 100 °C greater than bulk TEPA and also about 40 °C higher to TEPA@ActGO. The gradual decrease in stability with increasing loading agrees well with the facts of strong and weak pore confinement.

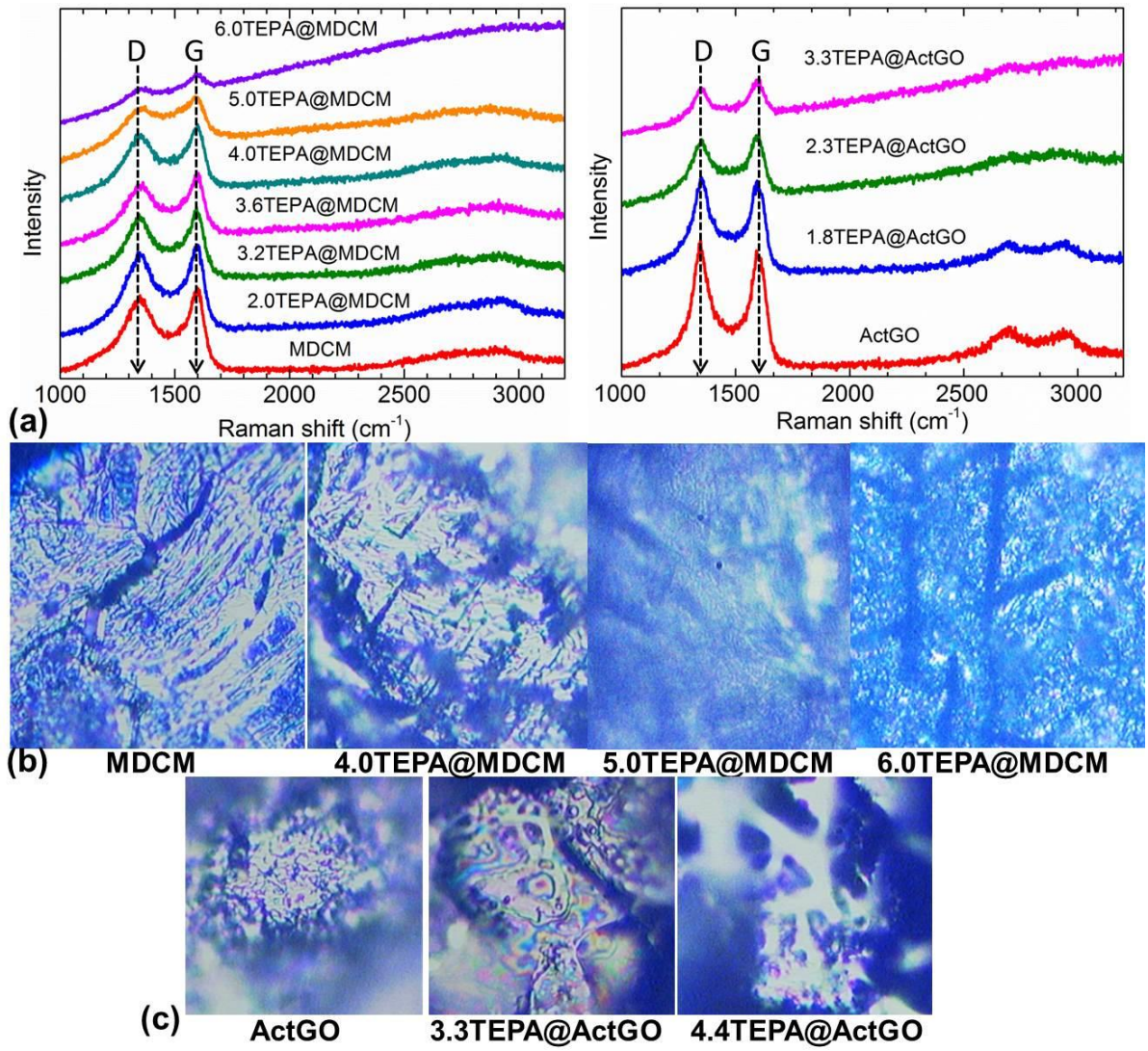

Figure S9. (a) Raman spectra of TEPA@MDCM (left) and TEPA@ActGO (right), (b) and (c) represent the optical images of the TEPA@MDCM and TEPA@ActGO, respectively, taken on the Raman instrument before recording the spectra. The optical images in ActGO clearly show the excess amine coating on the surface, whereas it is hardly seen in 6.0TEPA@MDCM sample. The increase in amine loading results in decreased peak (D and G modes) to background ratio. We are unable record a spectra on the 4.4TEPA@ActGO due to the large surface amine.

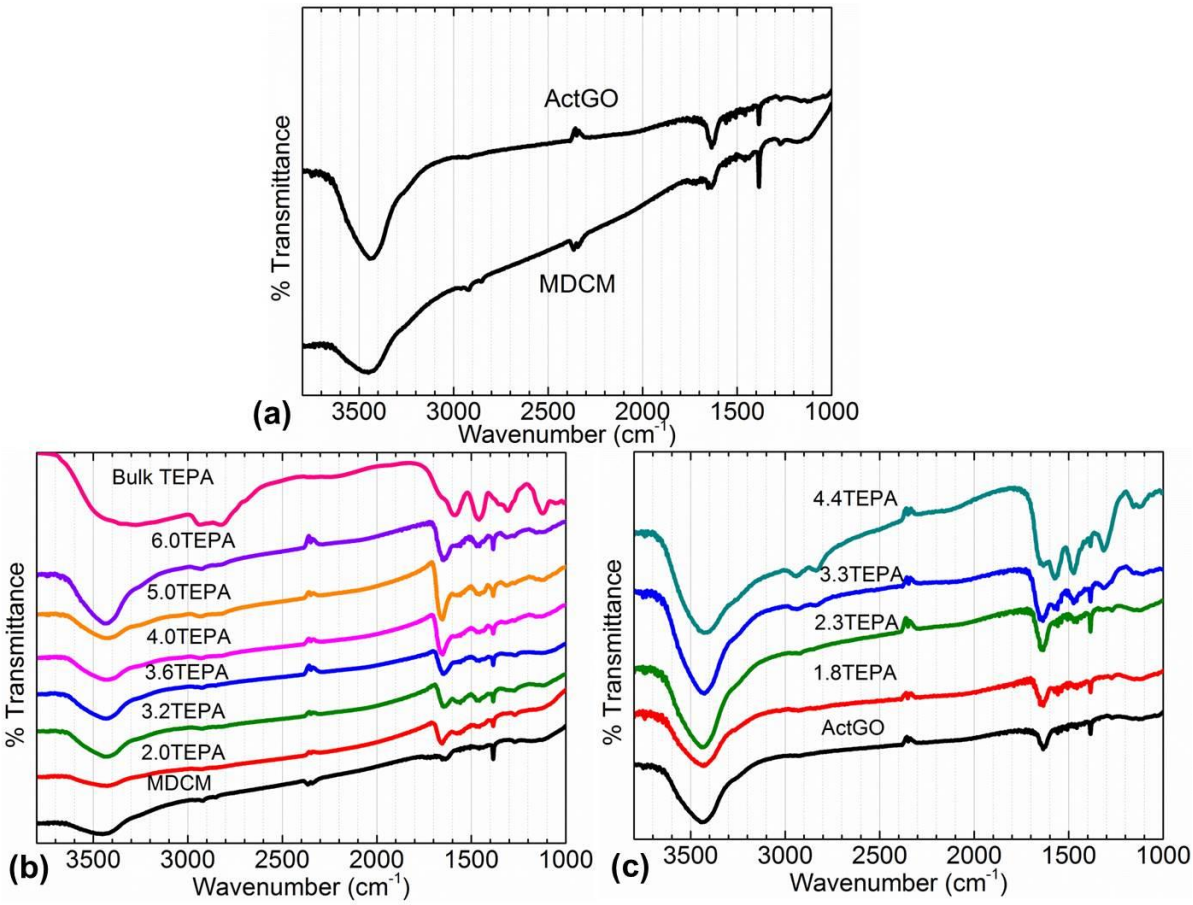

Figure S10. FTIR spectra of MDCM and ActGO before (a) and after (b-c) TEPA loading at different concentrations. The bulk TEPA is measured for a reference. In (a) FTIR spectrum of MDCM/ActGO shows a few vibrational modes at ca. 3444 cm^{-1} due to hydroxyl stretching vibrations in –COOH and/or adsorbed water, 1630 cm^{-1} owing to aromatic C=C/C=O stretching, ~1384 cm^{-1} correspond to O–H bending from hydroxyl/phenol groups and ~1272 cm^{-1} due to C–O–C stretching. For bulk TEPA, the IR absorption modes at ~3330 cm^{-1} and 1587 cm^{-1} correspond to N–H stretching and bending vibrations, while those at 2935 cm^{-1}, 2827 cm^{-1}, and 1459 cm^{-1} can be due to C–H stretching and bending vibrations, respectively. TEPA@MDCM shows some characteristic peaks of TEPA, such as the peaks at 2944 cm^{-1} (C–H), 2835 cm^{-1} (C–H), 1573 cm^{-1} (N–H) and 1471 cm^{-1} (C–H) indicating that TEPA has been impregnated onto support pores. It can be seen that the C–H modes of impregnated TEPA show a blue shift compared to that of free TEPA, while the N–H bands show a red shift.[32,33,37,38]

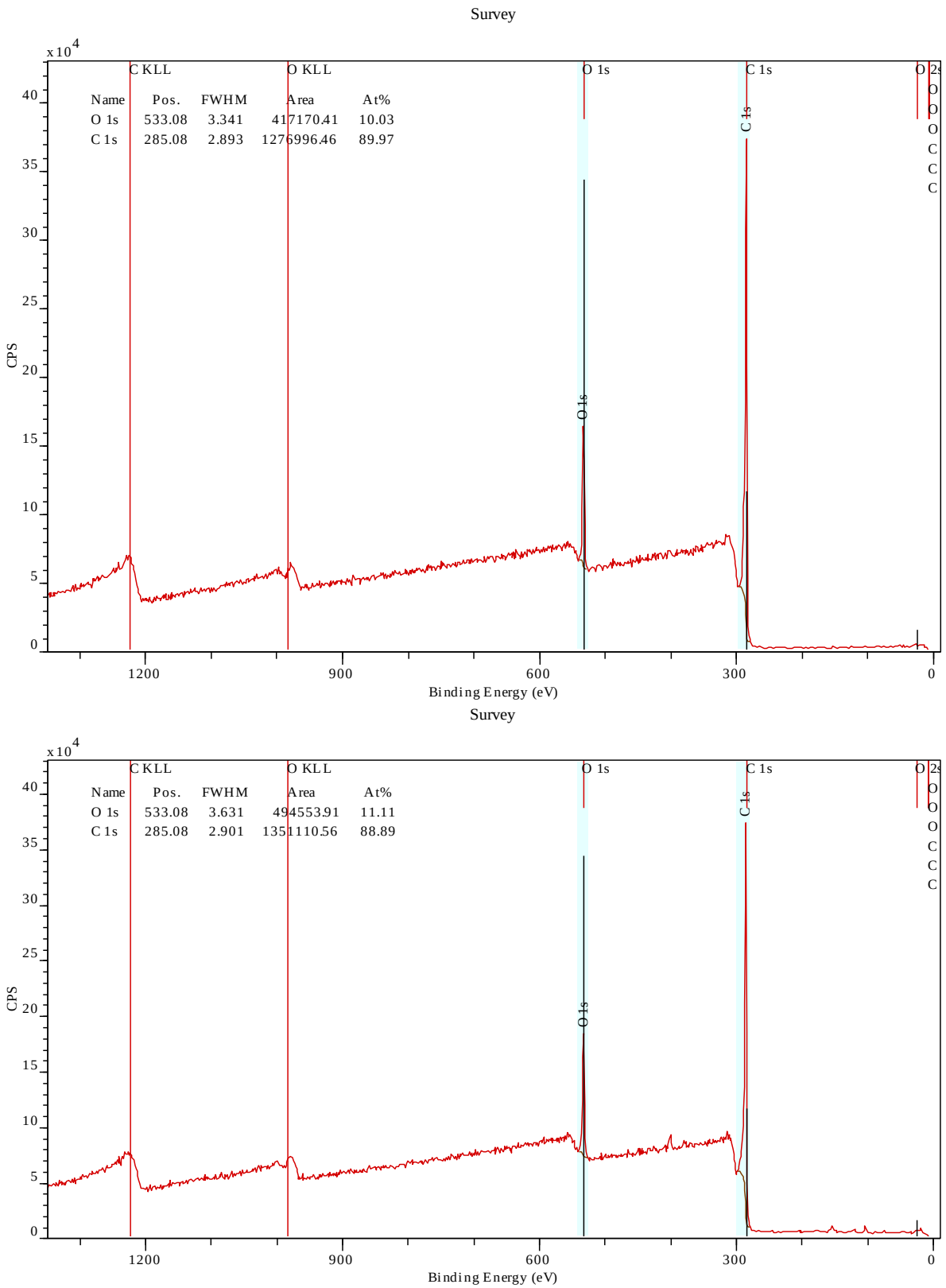

Figure S11a. XPS survey spectra of MDCM (above) and ActGO (below) accounts (89–90)% and (10–11)% of atomic carbon and oxygen, respectively.

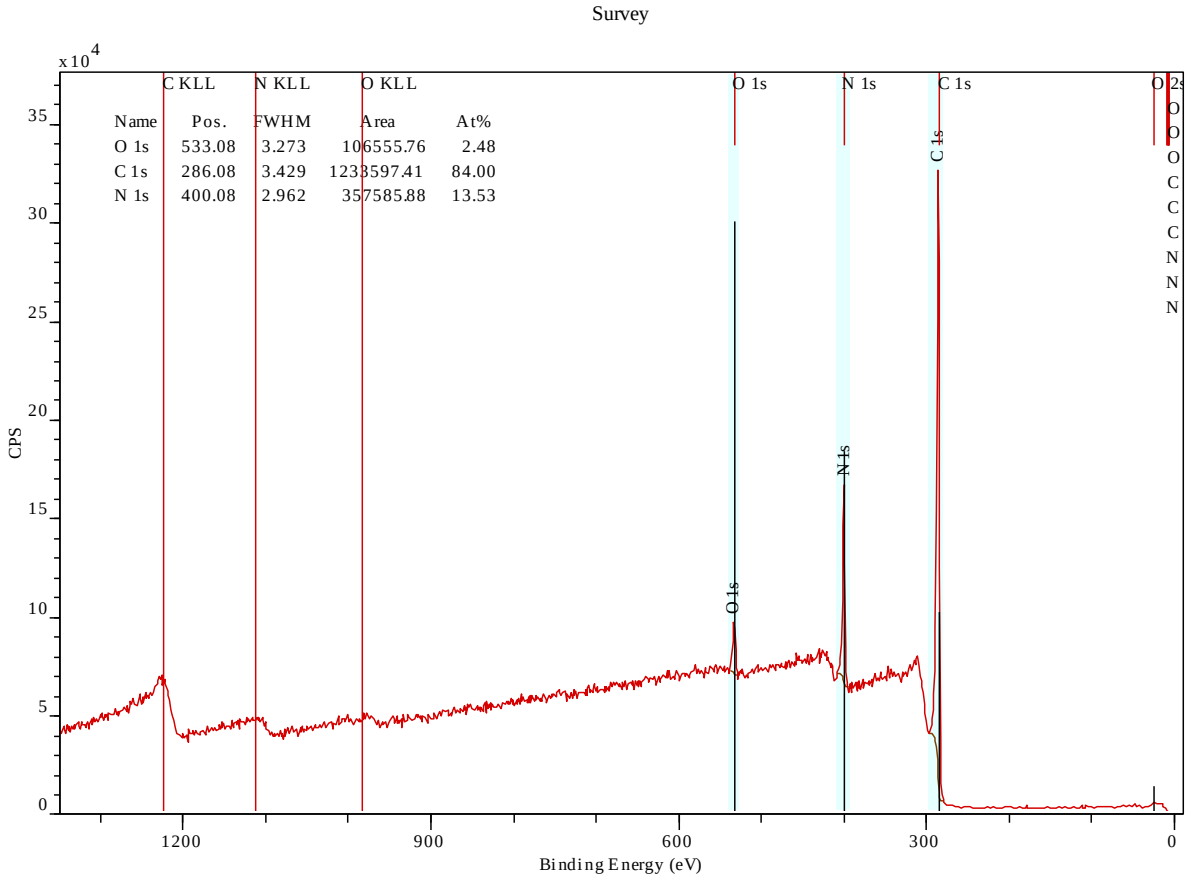

Figure S11b. XPS survey spectra of 4.0TEPA@MDCM accounts ~84%, ~13.5% and ~2.5% of atomic carbon, nitrogen and oxygen, respectively.

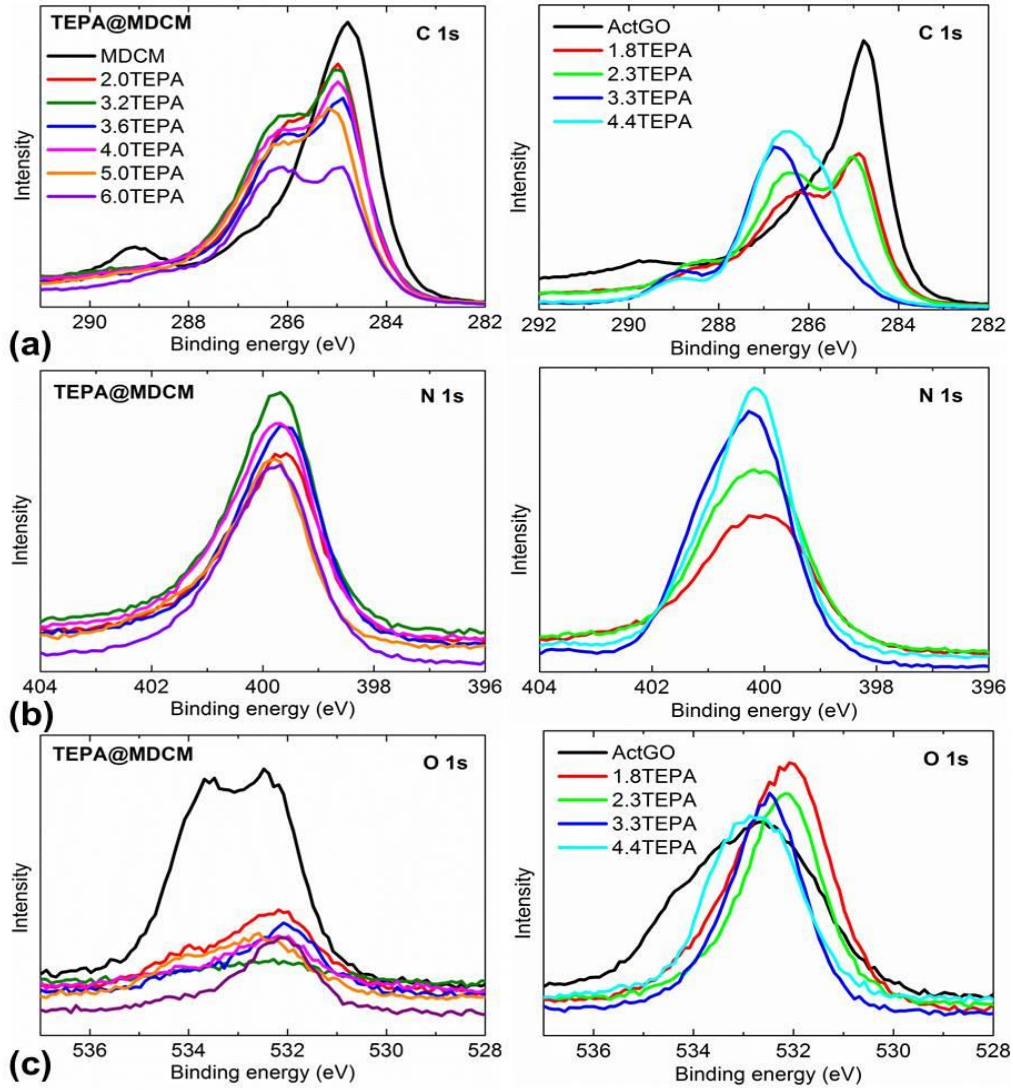

Figure S11c. XPS C 1s (a), N 1s (b) and O 1s (c) core level spectra of all the TEPA loaded MDCM (left panel) and ActGO (right panel) samples along with reference MDCM and ActGO. The deconvolution of C 1s core level spectrum of MDCM (Figure 2C) shows combination of graphitic sp^2 (C=C at 284.7 eV) and defective sp^3 (C–C at 285.5 eV) carbons with considerable oxygen functional groups; C–O and –COOH (or –OH–C=O) at 287.3 eV and 289.1 eV, respectively. This oxygen functionality is also seen in O 1s two peak behavior, which account equal portions of C–O at 532.3 eV and C–OH at 533.7 eV. After amine loading a clear change in C 1s and O 1s spectra is seen. A new shoulder appears at 285.8 eV due to the C–N bonds in the amine and above which the tail assigned to oxygen functionality and amide (NHC=O at ≥288 eV) formation between pore surface carbon and amine through oxygen.[39-41] Compared to MDCM samples, the completely buried sp^2 carbon of host is seen in 3.3TEPA and 4.4TEPA loaded ActGO samples due heavily covered surface excess TEPA. O 1s peaks become very week with most of the adsorbed oxygen (–OH) reduced and a shift of C–O to low binding energy suggest more coordinated oxygen between C and amine, could be a hydrogen bonded amines. Further to this the peak fitting of N 1s peak suggests more or less equal two peaks at ~399.6 eV and ~400.2 eV corresponding to amine ($–NH_2$) and amide (NHC=O) groups, respectively.

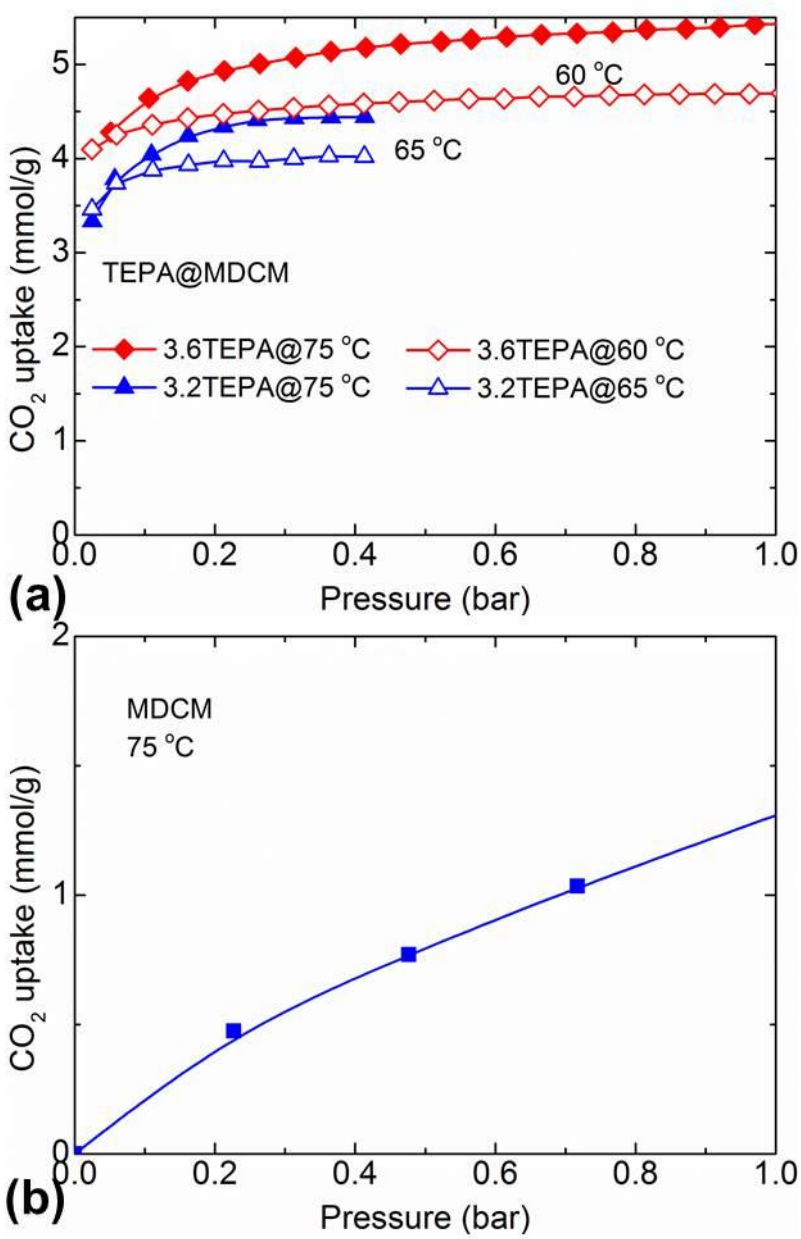

Figure S12. (a) Volumetric (60–75) °C CO_2 uptake isotherms of TEPA@MDCM, and (b) a 75 °C CO_2 uptake isotherm of MDCM. We also note that 75 °C is an optimum temperature for CO_2 uptake. A much lower, ~1.3 mmol g^{-1} (at 75 °C and 1 bar) of CO_2 uptake is observed in initial MDCM. The heat of adsorption in 3.6TEPA@MDCM and 3.2TEPA@MDCM is estimated according to the ref. 7 and found to be ~50 kJ mol^{-1} at low CO_2 uptake of 4.4 mmol g^{-1} and 3.7 mmol g^{-1}, respectively.

Table S2. Tabulated literature data on TEPA@silica; support porosity, total CO_2 uptake, experimental conditions (temperature & CO_2 concentration), capacity loss over repetitive cycles and corresponding reference. SSA & V_p are in $m^2\ g^{-1}$ & $cm^3\ g^{-1}$ of support, CO_2 uptake is in mmol g^{-1}, T is temperature in °C. The number in the parenthesis in %capacity loss column represents the number of cycles.

S/ No	Porosity of support		%TEPA/solid	CO_2 in	T	$\%CO_2$ content	%Capacity loss (vs number of cycles), desorption T	Year [Ref.]
	SSA	Vp						
1	272	1.08	60/sepiolite	2.2	60	1	-	2015 [11]
				3.8	60	1 & humid	14 (10), 90 °C des	
2	400	0.84	50/silica	3.45	75	10	5 (8), 100 °C des	2015 [42]
				4.28	75	10 & humid	-	
3	927	0.9	60/silica, MCM-41	2.45	70	15	-	2015 [43]
4	-	-	50/IG-MWCNT	3.1	75	10 & humid	1 (5), 150 °C des	2014 [44]
	-	-	50/silica, MCM-41	1.85	75	10 & humid	10 (5), 150 °C des	
5	316	0.77	50/bentonite clay	3.0	75	15	4.5 (10), 100 °C des	2013 [45]
				4.3	75	15 & humid	-	
6	808	1.5	50/silica nanotubes	3.58	75	10	3 (5), 100 °C des	2013 [46]
				4.74	75	10 & humid	-	
7	659	2.0	70/silica, MCF	4.57	75	10	3.5 (8), 100 °C des	2013 [37]
8	198	0.88	61/slica,TM2	4.0	75	10	5 (9), 100 °C des	2013 [47]
	6	0.03	55/silica, IM15	2.45	75	10	23 (9), 100 °C des	
9	302	0.96	50/TiO_2 nanotubes	4.0	70	15	5 (10), 100 °Cdes	2013 [48]
10	272	1.54	70/silica, MSU-F	4.17	40	100	-	2013 [49]
11	780	0.21	40/MOF-74	6	60	15	3 (5), 100 °C des	2013 [50]
12	302	0.96	69/TiO_2 nanotubes	4.37	60	15	4 (5), 100 °C des	2013 [28]
				5.24	60	15 & humid	13 (5), 100 °C des	
13	500	1.2	38/silica, Diaion™	3.9	40	15	-	2012 [51]
	300	1.15	36/silica, Davisil	2.6	40	15	-	
	263	1.24	39/silica, Q-10	2.3	40	15	-	
	663	0.43	13/silica, Q-3	0.6	40	15	-	
14	900	0.97	50/silica	3.86	75	100	-	2012 [52]
15	725	0.73	83/silica capsule	5.57	75	10	39 (50), 100 °C des	2011 [18]
	881	0.64	50/silica, MSU-1	3.4	75	10	-	2011 [53]
16	14	0.08	50/silica, MSU-1	3.9	75	10	13 (12), 100 °C des	
	-	-	50/silica, KIT-6	2.85	60	10	-	2011 [54]
17				3.2	60	10 & humid	1.5 (10), 120 °C des	
	118	0.31	50/silica, SBA-15	4.6	75	15	2 (10), 75 °C des	2011 [55]
18				5.0	75	15 & humid	-	
19	943	1.0	50/silica, KIT-6	2.9	60	10	5 (40), 100 °C des	2010 [56]
20	523	1.13	40/silica monolith	3.9	75	100	8 (5), 100 °C des	2010 [57]
	54	0.4	50/silica, MSFas	4.1	75	15	20 (7), 75 °C des	2010 [58]
21				5.3	75	15 & humid	-	
	975	0.3	50/zeolite, Y60	2.6	60	15	12 (20), 75 °C des	2010 [59]
22				4.3	60	15 & humid	-	
	1101	0.96	50/silica, MCM-41	0.9	25	100	-	2010 [60]
23	1124	0.98	50/silica, MCM-48	0.7	25	100	-	
	712	0.68	50/silica, SBA-15	0.7	25	100	-	
24	950	3.2	65/silica monolith	5.9	75	100	8 (5), 75 °C des	2009 [20]
25	16	0.03	50/silica, MCM-41	4.8	75	100	11 (6), 100 °C des	2008 [29]
26	345	0.71	70/silica, SBA-15	3.9	75	100	8 (7), 100 °C des	2006 [30]

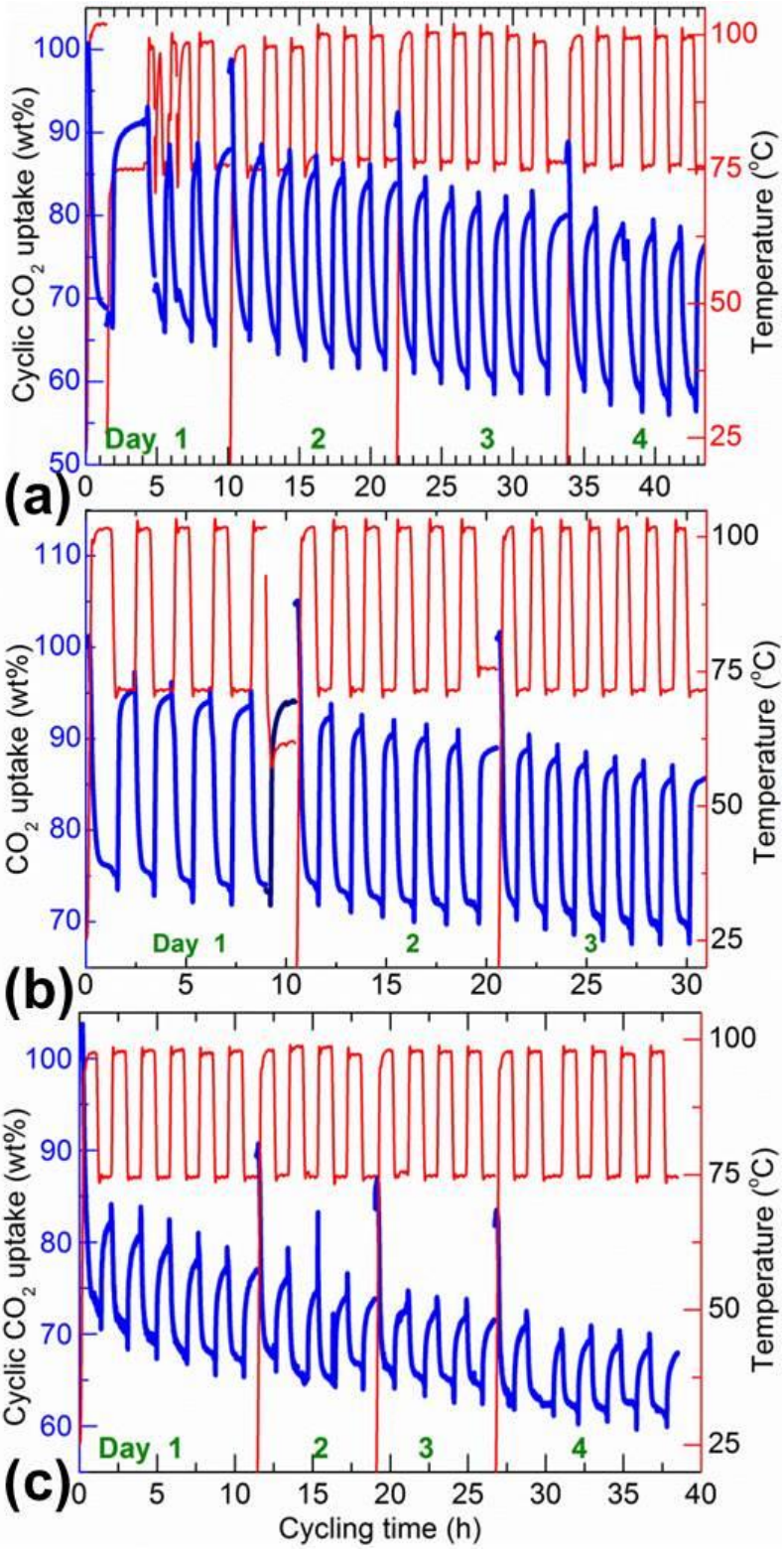

Figure S13. TG cyclic CO_2 uptake runs at 75 °C on 5.0TEPA@MDCM (a), 6.0TEPA@MDCM (b) and 4.4TEPA@ActGO (c). In all 3 cases the test runs were measured at similar conditions with 50 min each sorption-desorption (at 100 °C) under flowing 15% CO_2 (balanced with N_2) through a water bubbler at ~50 ml min^{-1}.

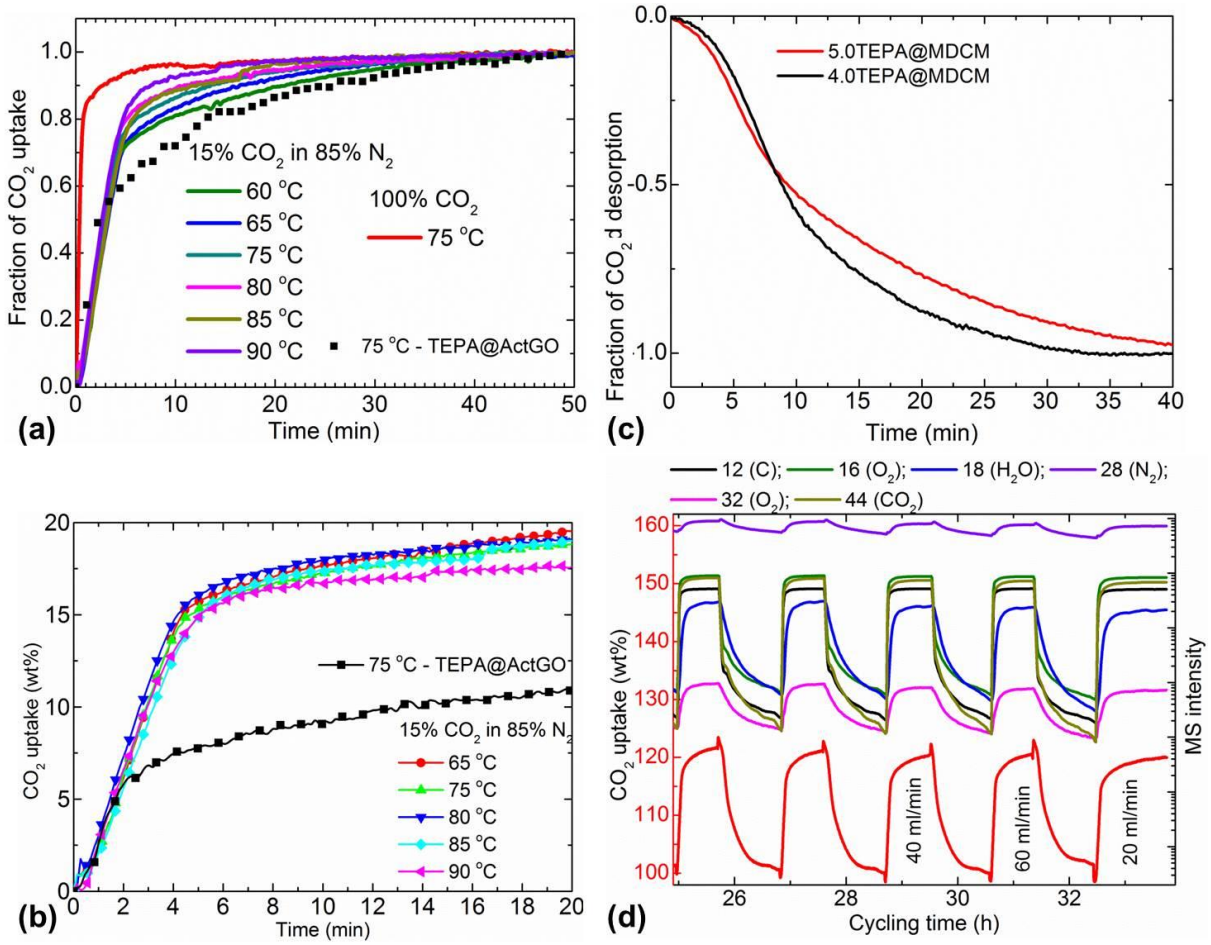

Figure S14. Left: Temperature dependent, humidified CO_2 uptake and kinetics of 5.0TEPA@MDCM and 4.4TEPA@ActGO, measured on TG. One can see that the uptake kinetics in TEPA@ActGO is much slower compared with TEPA@MDCM at the same experimental conditions, 75 °C with 15% CO_2. **Right:** (c) Desorption kinetics of 4.0TEPA@MDCM and 5.0TEPA@MDCM samples at ~100 °C under dry N_2 flow suggests that the more loading of amine exhibits slow desorption kinetics. (d) Mass spectroscopy (MS) during the TG cyclic CO_2 uptake test runs of 5.0TEPA@MDCM, performed at different flow rates (20 ml/min to 60 ml/min) of CO_2 bubbled through water bubbler. MS signals at desorption cycles suggest formation of ammonium bicarbonate under humid conditions (Scheme S2). When looked at uptake and desorption kinetics with fast initial kinetics followed by slow equilibrium, it is understood that a mixture of ammonium carbamate (Scheme S1) and bicarbonate formation occurs. It is argued that ammonium carbamate formation occurs at a much faster rate than bicarbonate formation. As a result, the reaction can take a very long time to reach a full equilibrium capacity in the presence of H_2O.[61]

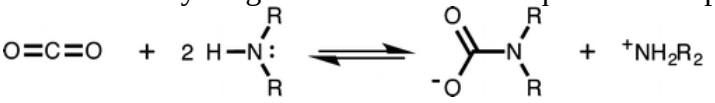

Scheme S1. Under Dry Conditions, Reaction of CO_2 with 2 equiv of a 1° or 2° Alkylamine Amine Typically Forms Ammonium Carbamate.

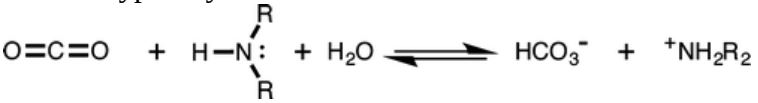

Scheme S2. Under Humid Conditions, Reaction of CO_2 with 1 equiv of a 1° or 2° Alkylamine Typically Forms Ammonium Bicarbonate.

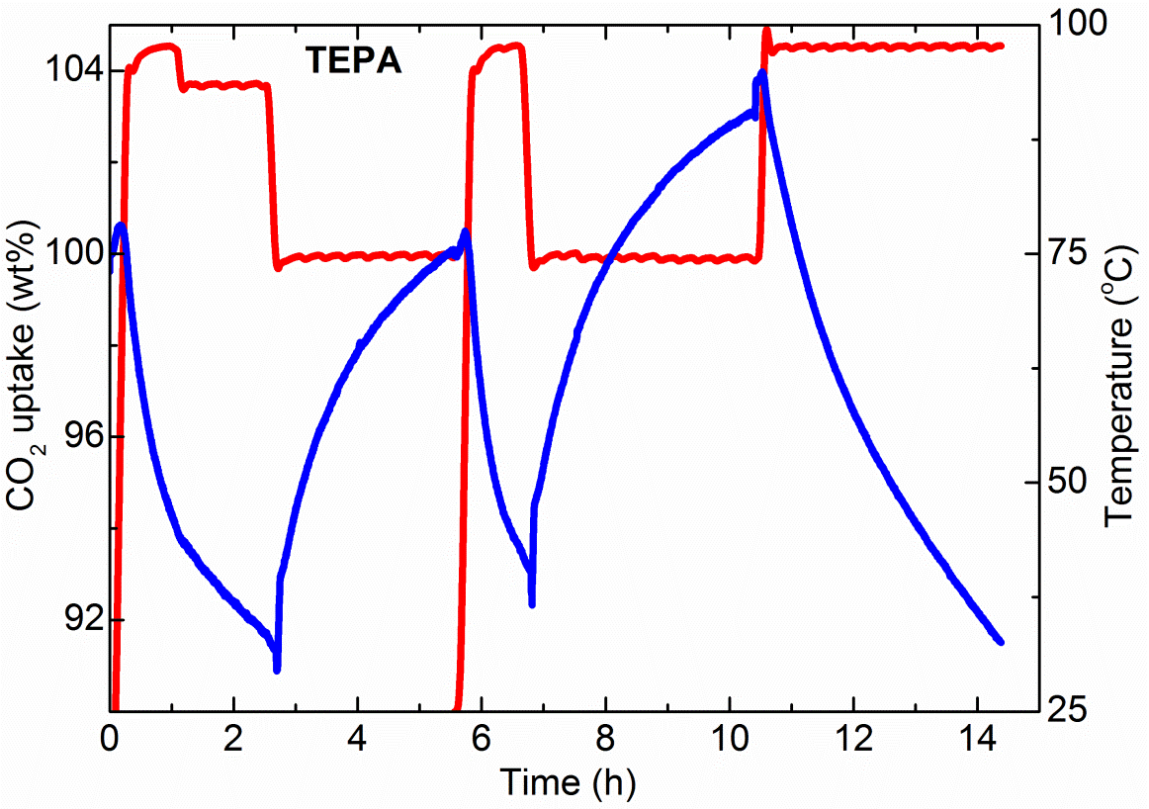

Figure S15. Humidified 15% CO_2 (in 85%N_2) uptake and kinetics of bulk TEPA at 75 °C.

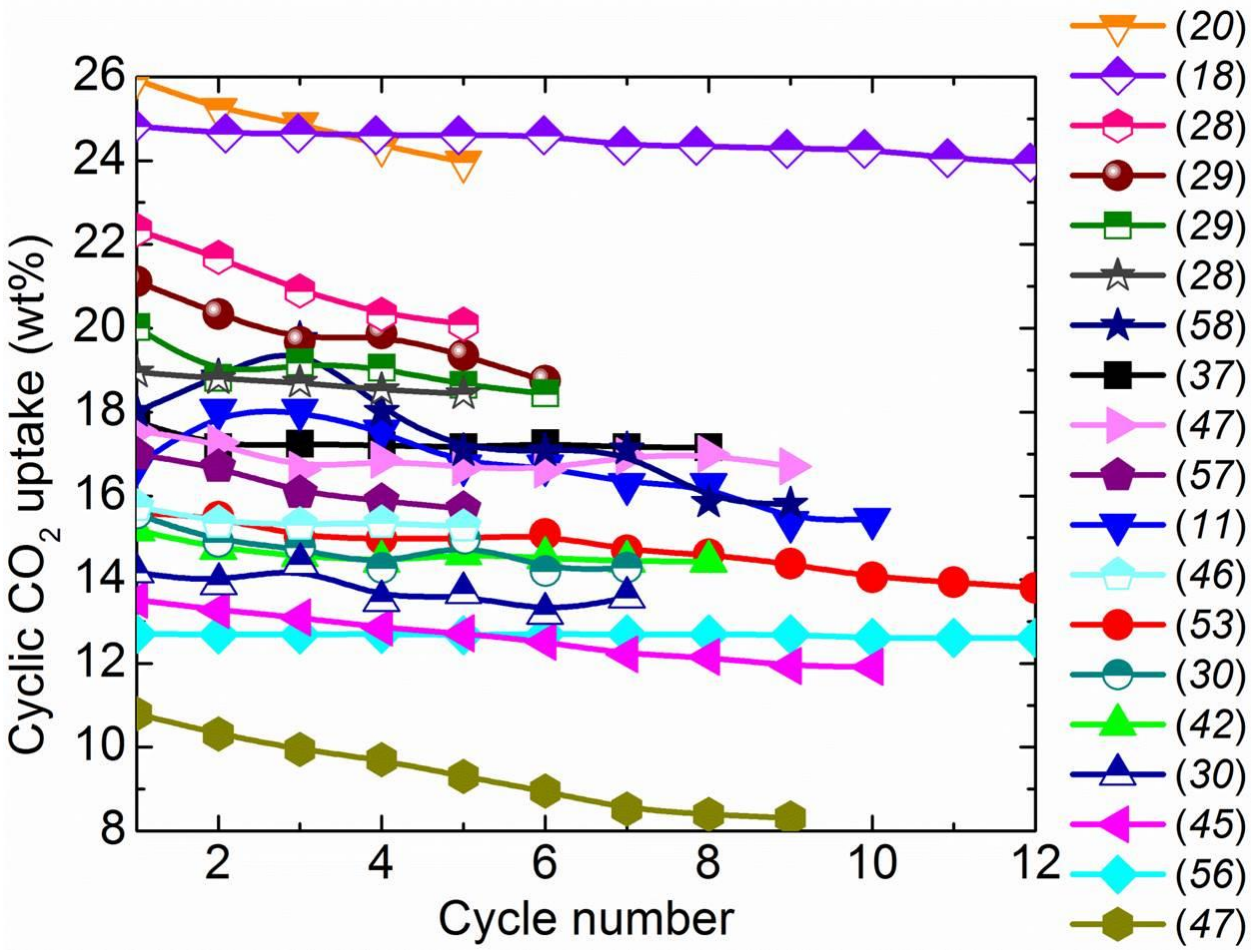

Figure S16. CO_2 uptake capacity stability against number of cyclic runs of literature reference (in parenthesis) data on TEPA loaded solids.

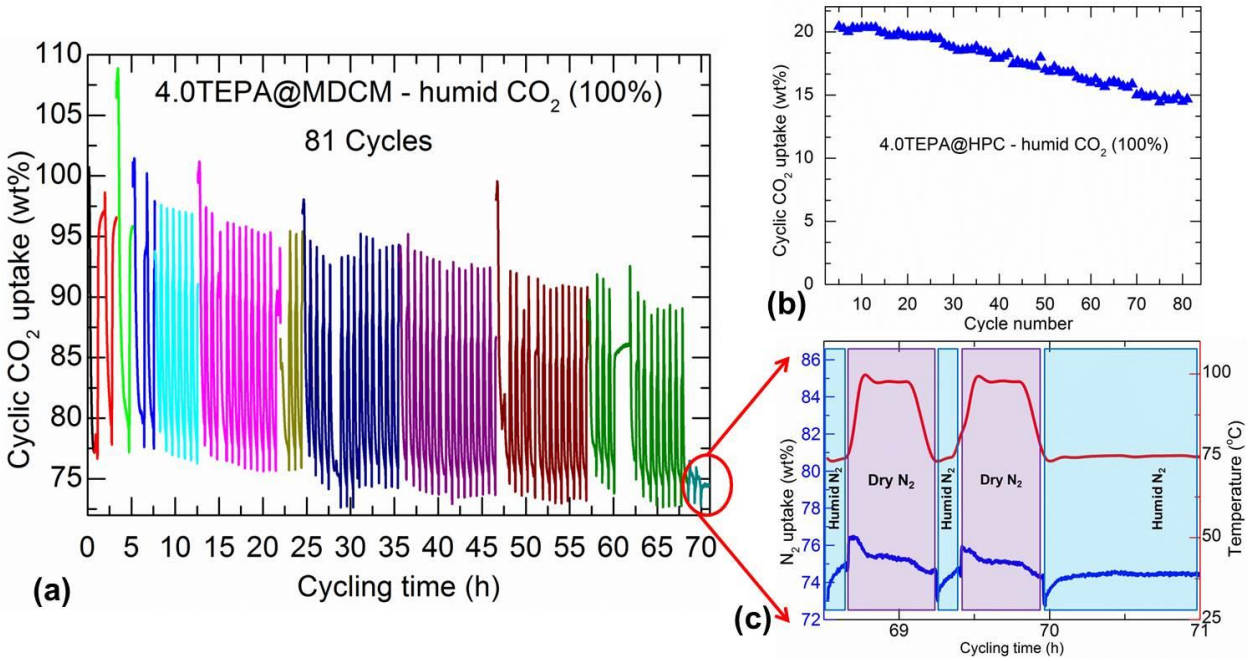

Figure S17. (a) Humidified, 100% CO_2 uptake life cycle cycling test runs of 4.0TEPA@MDCM with 10 min and 20 min sorption and desorption runs at 75 °C and 100 °C, respectively. (b) CO_2 uptake cyclic stability against number of cyclic runs. (c) Humidified, 100% N_2 uptake cycling runs at similar conditions of CO_2 cyclic runs.

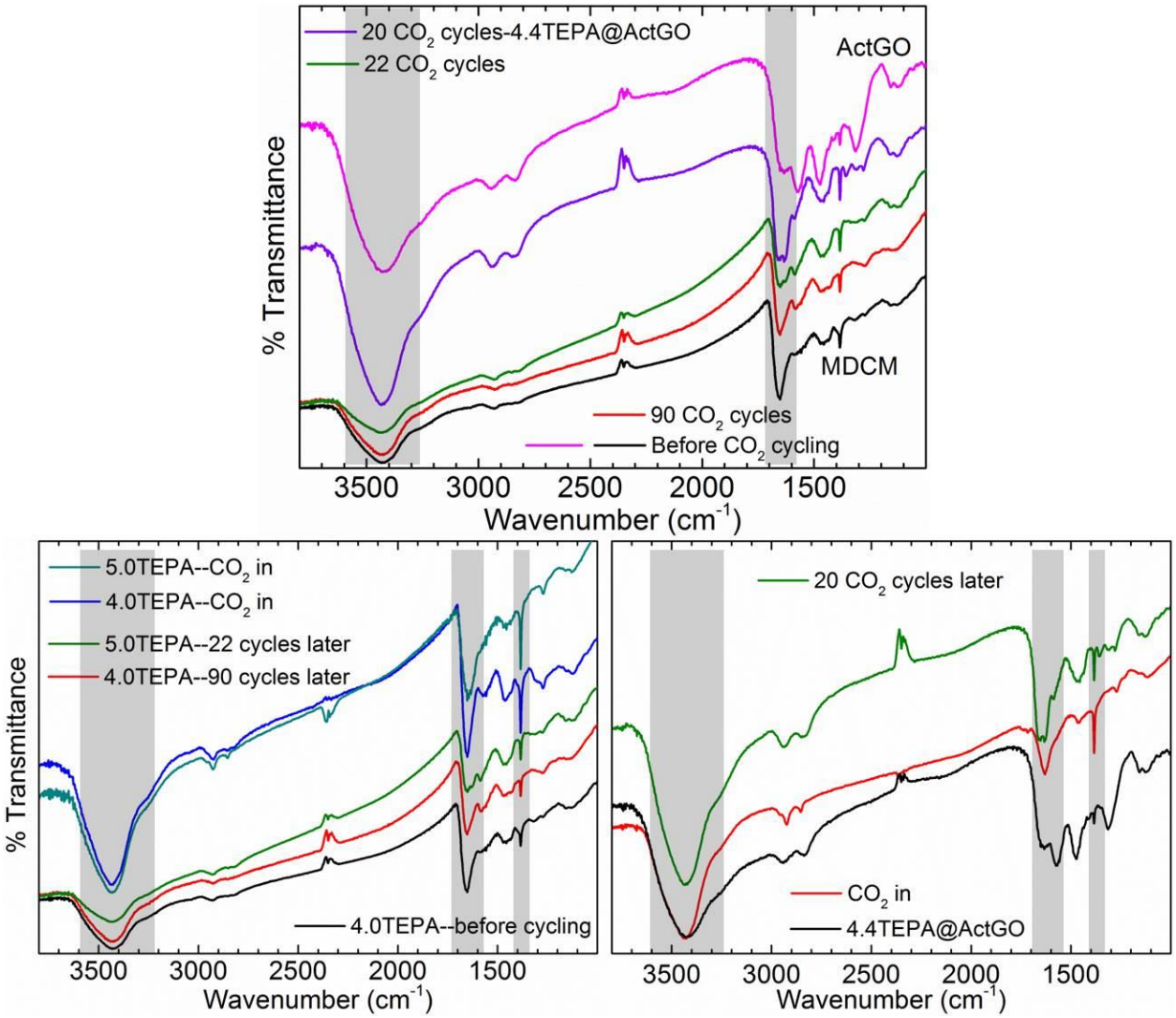

Figure S18. FTIR spectra of TEPA loaded MDCM and ActGO after CO_2 uptake and cyclic test runs. Top: after cyclic runs with CO_2 desorbed state. Bottom-left: before and after initial CO_2 uptake and cyclic test runs with CO_2 desorbed state in TEPA@MDCM. Bottom-right: 4.4TEPA@ActGO before and after initial CO_2 adsorption, and after 22 cyclic runs with CO_2 desorbed state. The highlighted regions of the spectra shows the relative changes in the –OH, C=C/C=O stretches before and after CO_2 uptake and cyclic test runs. The partial oxidation of the samples is see through the enhanced IR adsorption peak intensity/broadening around (1630-1660) cm^{-1}.[32,33] A relatively very high intense IR peaks at (3300-3600) cm^{-1} and 1384 cm^{-1} are seen in the samples after humidified CO_2 uptake (see bottom figures), is consistent with extra added –OH and C=O groups from the feed gas stream.

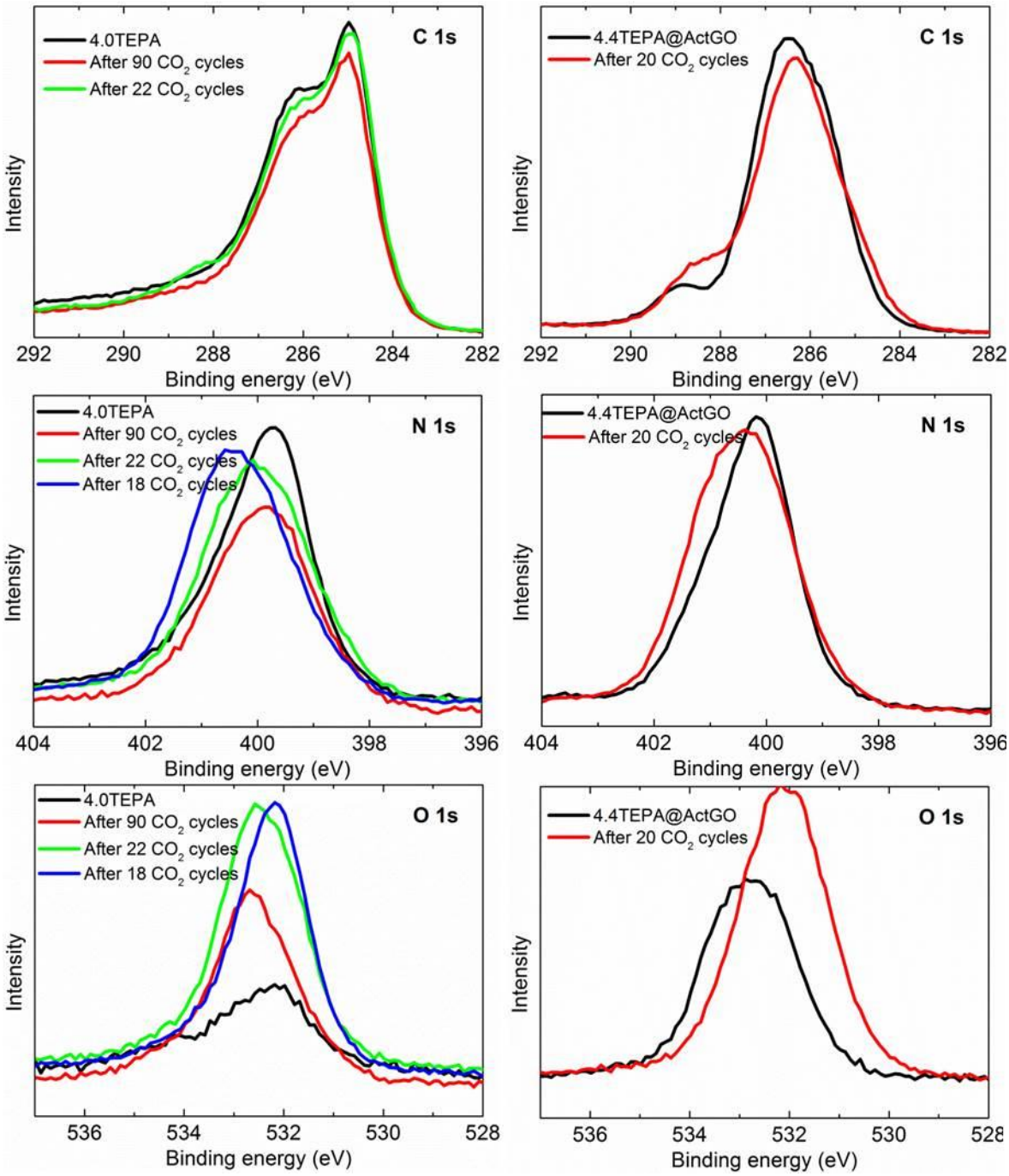

Figure S19. XPS spectra of the samples after subjecting to CO_2 cyclic test runs. The partial oxidation of the samples is seen at C 1s with a little shoulder above 288 eV. Furthermore clear shifts in N 1s and O 1s peaks to higher binding energies are consistent with oxidation of amines.[39-41] The tendency of oxidation is more with increased TEPA loading and it is in the order of 6.0TEPA@MDCM (for 18 cycles) > 5.0TEPA@MDCM for 22 cycles > 4.0TEPA@MDCM for 90 cycles.

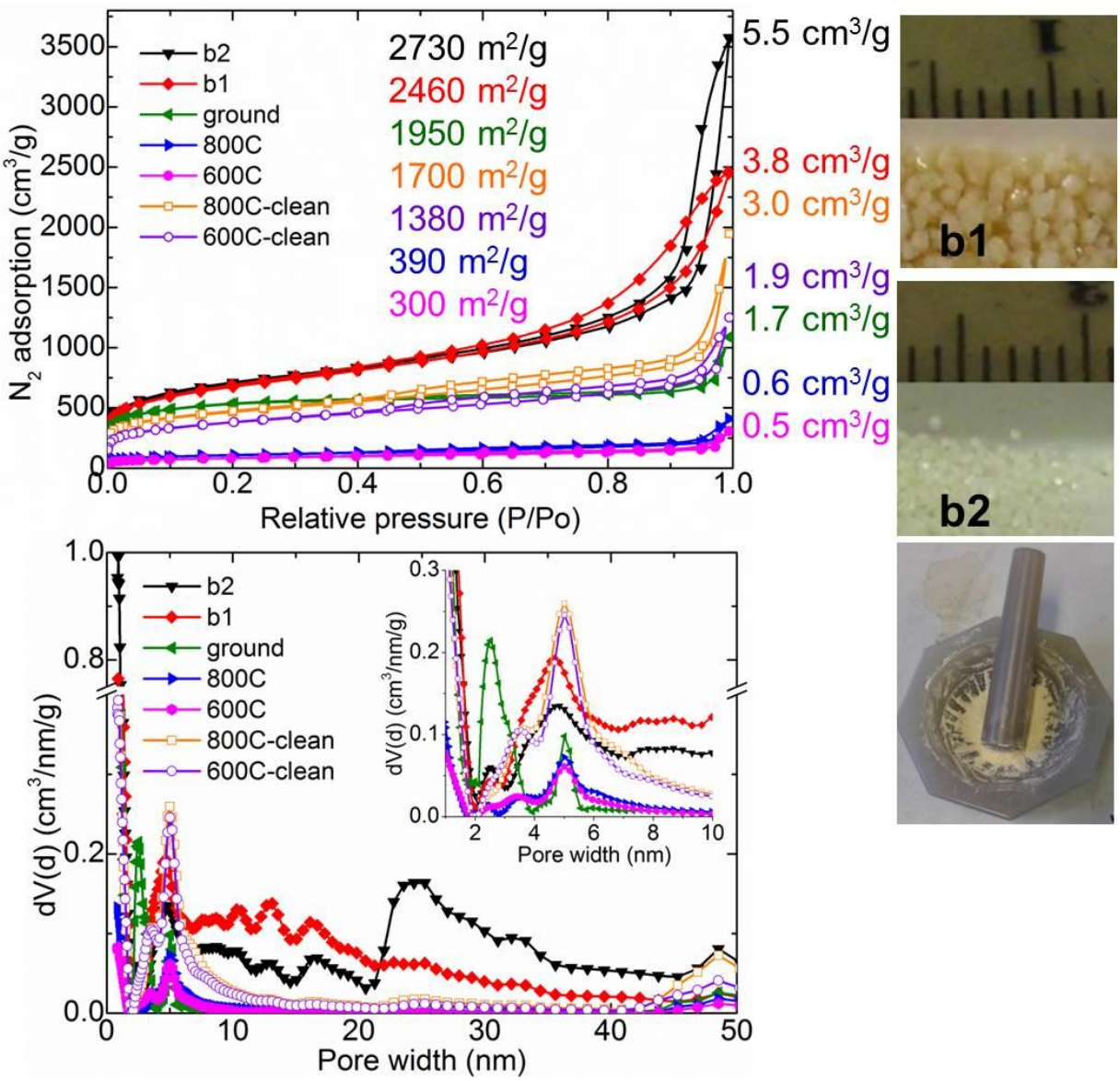

Figure S20. Control over porosity in MDCM. Top: 77 K N_2 adsorption isotherms of MOF-5 derived carbons from different MOF crystal sizes and different carbonization temperatures. The lables, b1, b2 and ground are 1000 °C carbonized and 600C, 800C represent the as-synthesized carbons at 600 °C and 800 °C. 600C-clean and 800C-clean are after acid treatment to remove ZnO in the carbon network. All the sample are carbonized for 6 h under N_2 flow. Bottom: the pore-size distribution plots of respective N_2 isotherms derived by applying QSDFT model fiting. Right: MOF-5 with different crystal sizes. Clearly the large crystals show highest total pore volume of 5.5 $cm^3\ g^{-1}$ [ref. 23] and is considerably reduced with the small (3.8 $cm^3\ g^{-1}$) [ref. 23] and ground (1.7 $cm^3\ g^{-1}$) MOF-5 crystals. A limited pore-sizes and its distribution is seen in smaller crystals than the millimetre sized crystals. The 800C sample after acid treatment shows reasonably high mesopore total pore volume of 3.0 $cm^3\ g^{-1}$ with most of the pore situated around 6 nm and distributed within (2-10) nm. This could be advantageous in enhancing the amine efficiency.

References

35. S. Gadipelli, Z. X. Guo, Postsynthesis annealing of MOF-5 remarkably enhances the framework structural stability and CO_2 uptake, *Chem. Mater*. **26**, 6333-6338 (2014).
36. G. Srinivas, J. Burres, T. Yildirim, Graphene oxide derived carbons (GODCs): Synthesis and gas adsorption properties. *Energy Environ. Sci.* **5**, 6453-6459 (2012).
37. X. Feng, G. Hu, X. Hu, G. Xie, Y. Xie, J. Lu, M. Luo, Tetraethylenepentamine-modified siliceous mesocellular foam (MCF) for CO_2 capture, *Ind. Eng. Chem. Res*. **52**, 4221-4228 (2013).
38. J. Joseph, E. D. Jemmis, Red-, blue-, or no-shift in hydrogen bonds: A unified explanation, *J. Am. Chem. Soc*. **129**, 4621-4632 (2007).
39. T. Ramanathan, F. T. Fisher, R. S. Ruoff, L. C. Brinson, Amino-functionalized carbon nanotubes for binding to polymers and biological systems, *Chem. Mater*. **17**, 1290-1295 (2005).
40. N. Graf, E. Yegen, T. Gross, A. Lippitz, W. Weigel, S. Krakert, A. Terfort, W. E.S. Unger, XPS and NEXAFS studies of aliphatic and aromatic amine species on functionalized surfaces, *Surf. Sci*. **603**, 2849-2860 (2009).
41. E. P. Dillon, E. Andreoli, L. Cullum, A. R. Barron, Polyethyleneimine functionalised nanocarbons for the efficient adsorption of carbon dioxide with a low temperature of regeneration, *J. Experimental Nanoscale*, DOI: 10.1080/17458080.2014.894256 (2014).
42. L. Wang, M. Yao, X. Hu, G. Hu, J. Lu, M. Luo, M. Fan, Amine-modified ordered mesoporous silica: The effect of pore size on CO_2 capture performance, *Appl. Sur. Sci*. **324**, 286-292 (2015).
43. X. Wang, L. Chen, Q. Guo, Development of hybrid amine-functionalized MCM-41 sorbents for CO_2 capture, *Chem. Eng. J*. **260**, 573-581 (2015).
44. Q. Liu, B. Xiong, J. Shi, M. Tao, Y. He, Y. Shi, Enhanced tolerance to flue gas contaminants on carbon dioxide capture using amine-functionalized multiwalled carbon nanotubes, *Energy Fuels* **28**, 6494-6501 (2014).
45. W. Wang, X. Wang, C. Song, X. Wei, J. Ding, J. Xiao, Sulfuric acid modified bentonite as the support of tetraethylenepentamine for CO_2 capture, *Energy Fules* **27**, 1538-1546 (2013).
46. M. Yao, Y. Dong, X. Hu, X. Feng, A. Jia, G. Xie, G. Hu, J. Lu, M. Luo, M. Fan, Tetraethylenepentamine-modified silica nanotubes for low-temperature CO_2 capture, *Energy Fuels* **27**, 7673-7680 (2013).
47. Y. Li, X. Wen, L. Li, F. Wang, N. Zhao, F. Xiao, W. Wei, Y. Sun, Synthesis of amine-modified mesoporous materials for CO_2 capture by a one-pot template-free method, *J. Sol-Gel Sci. Technol*. **66**, 353-362 (2013).
48. F. Song, Y. Zhao, Q. Zhong, Adsorption of carbon dioxide on amine-modified TiO_2 nanotubes, *J. Environ. Sci*. **25**, 554-560 (2013).
49. D. S. Dao, H. Yamada, K. Yogo, Large-pore mesostructured silica impregnated with blended amines for CO_2 capture, *Ind. Eng. Chem. Res*. **52**, 13810-13817 (2013).
50. Y. Cao, F. Song, Y. Zhao, Q. Zhong. Capture of carbon dioxide from flue gas on TEPA-grafted metal-organic framework Mg_2(dobdc), *J. Environ. Sci*. **25**, 2081-2087 (2013).

51. R. Veneman, Z. S. Li, J. A. Hogendoorn, S. R. A. Kersten, D. W. F. Brilman, Continuous CO_2 capture in a circulating fluidized bed using supported amine sorbents, *Chem. Eng. J.* **18-26**, 207-208 (2012).

52. J. Yu, Y. Le, B. Cheng, Fabrication and CO_2 adsorption performance of bimodal porous silica hollow spheres with amine-modified surfaces, *RSC Adv*. **2**, 6784-6791 (2012).

53. X. Wang, H. Li, H. Liu, X. Hou, As-synthesized mesoporous silica MSU-1 modified with tetraethylenepentamine for CO_2 adsorption, *Microp. Mesop. Mater*. **142**, 564-569 (2011).

54. Y. Liu, Q. Ye, M. Shen, J. Shi, J. Chen, H. Pan, Y. Shi, Carbon dioxide capture by functionalized solid amine sorbents with simulated flue gas conditions, *Environ. Sci. Technol*. **45**, 5710-5716 (2011).

55. S.-H. Liu, Y.-C. Lin, Y.-C. Chien, H.-R. Hyu, Adsorption of CO_2 from flue gas streams by a highly efficient and stable aminosilica adsorbent, *J. Air & Waste Manag. Assoc*. **61**, 226-233 (2011).

56. Y. Liu, J. Shi, J. Chen, Q. Ye, H. Pan, Z. Shao, Y. Shi, Dynamic performance of CO_2 adsorption with tetraethylenepentamine-loaded KIT-6, *Microp. Mesop. Mater*. **134**, 16-21 (2010).

57. J. J. Wen, F. N. Gu, F. Wei, Y. Zhou, W. G. Lin, J. Yang, J. Y. Yang, Y. Wang, Z. G. Zou, J. H. Zhu, One-pot synthesis of the amine-modified meso-structured monolith CO_2 adsorbent, *J. Mater. Chem*. **20**, 2840-2846 (2010).

58. S.-H. Liu, C.-H. Wu, H.-K. Lee, S.-B. Liu, Highly stable amine-modified mesoporous silica materials for efficient CO_2 capture, *Top. Catal*. **53**, 210-217 (2010).

59. F. Su, C. Lu, S.-C. Kuo, W. Zeng, Adsorption of CO_2 on amine-functionalized Y-type zeolites, *Energy Fules* **24**, 1441-1448 (2010).

60. M. Bhagiyalakshmi, L. J. Yun, R. Anuradha, H. T. Jang, Utilization of rice husk ash as silica source for the synthesis of mesoporous silicas and their application to CO_2 adsorption through TREN/TEPA grafting, *J. Hazar. Mater*. **175**, 928-938 (2010).

61. J. A. Mason, T. M. McDonald, T.-H. Bae, J. E. Bachman, K. Sumida, J. J. Dutton, S. S. Kaye, J. R. Long, Application of a High-Throughput Analyzer in Evaluating Solid Adsorbents for Post-Combustion Carbon Capture via Multicomponent Adsorption of CO_2, N_2, and H_2O. *J. Am. Chem. Soc.*, **137**, 4787–4803 (2015).